1979

The crystal and molecular structures of some organophosphorus insecticides and computer methods for structure determination

Ricky Lee Lapp
Iowa State University

The crystal and molecular structures of some organophosphorus insecticides and computer methods for structure determination

by

Ricky Lee Lapp

A Dissertation Submitted to the
Graduate Faculty in Partial Fulfillment of the
Requirements for the Degree of
DOCTOR OF PHILOSOPHY

Department: Chemistry
Major: Physical Chemistry

Approved;

Signature was redacted for privacy.

In Charge of Major Work

Signature was redacted for privacy.

For the Major Department

Signature was redacted for privacy.

For the Graduate College

Iowa State University
Ames, Iowa

1979

TABLE OF CONTENTS

INTRODUCTION TO ORGANOPHOSPHORUS INSECTICIDES

Acetylcholinesterase (AChE), one of the hydrolytic enzymes for acetylcholine, is the target of organophosphorus esters, including insecticides and nerve gases. The inhibition of the enzyme disturbs the normal operation of the nervous system, finally resulting in the death of the subject. The neuron consists of an elongated axon and short branched dendrites. The axon ending connects with another neuron through a synapse, or with a muscular fiber through the neuromuscular junction. The nerve membrane covering the axon has a selective permeability to ions and normally the potassium ion concentration is higher inside the axon than out, while the reverse is true for sodium ions. Owing to the concentration gradients of these ions, the resting nerve membrane is polarized at the equilibrium potential.

About every micrometer along the axon there are clusters of tiny vesicles each containing on the order of 10,000 molecules of acetylcholine. On the opposite side of the synaptic cleft (200 to 300 Å in interneuron synapses and 500 to 600 Å in neuromuscular junctions) are the acetylcholine receptors. An impulse arriving at the presynaptic membrane induces several hundred synaptic vesicles to release acetylcholine into the synaptic cleft. The acetylcholine diffuses rapidly across the cleft and combines with the receptor molecules where it causes channels to open in the cell

membrane allowing sodium to enter the cell and potassium to leave. The resulting electric current short-circuits the normal potential across the resting cell membrane. This depolarization produces the excitatory postsynaptic potential or end-plate potential. When the potential achieves a threshold, an action potential rises rapidly to excite the neuron or muscle fiber.

Acetylcholine would remain in the synaptic cleft, moving from one receptor molecule to another and opening additional channels, if it were not for the enzyme acetylcholinesterase which rapidly hydrolyzes acetylcholine into acetic acid and choline. Most acetylcholinesterase is localized near the receptors on the postsynaptic membrane. As long as acetylcholine remains in the region of the synaptic cleft, the original state of the postsynaptic membrane cannot be reestablished. Therefore, the inhibition of AChE leads to a disturbance of the nervous function which leads to severe and often lethal damage in the organism.

The inhibition of AChE by organophosphate esters is based on phosphorylation of an active enzyme site which is then unable to bind the natural substrate, i.e.

$$(RO)_2POX + EH \longrightarrow (RO)_2POE + HX$$

where X is the "leaving group" on the ester and EH is the uninhibited AChE. Unlike the acetylated AChE, which is unstable and hydrolyzed very rapidly, the phosphorylated

enzyme is very stable and its generation lowers the concentration of AChE available for binding acetylcholine. With a sufficiently high insecticide concentration ($\sim 10^{-6}$ to 10^{-9}M), the nonphosphorylated AChE is eventually unable to hydrolyze the acetylcholine being constantly produced during synaptic transmission.

The phosphorylation is due in part to structural and chemical similarities between acetylcholine and organophosphorus (OP) insecticides. The phosphate ester binds to the esteratic site of AChE in place of the acetyl group of acetylcholine. Some portion of the leaving group binds to the anionic site of AChE in place of the quaternary nitrogen of acetylcholine. Determining the relationship between structure and effectiveness of OP insecticides, therefore, requires a close examination of structural parameters to develop models for AChE enzyme surfaces and to determine the nature of the active sites.

THE CRYSTAL AND MOLECULAR STRUCTURE OF DIMETHOATE

Introduction

Dimethoate is a highly species specific insecticide with a toxicity ratio (LD_{50} mouse/LD_{50} housefly) of 280 and an oral LD_{50} for rats of over 600 mg/kg. It also contains several structural similarities to azinphos-methyl[1] (LD_{50} = 16 mg/kg) and amidithion[2] (LD_{50} = 600 mg/kg), which have been previously studied in this laboratory. For these reasons a crystal of dimethoate (dimethyl S-(N-methylcarbamoylmethyl) phosphorodithioate) was selected for three-dimensional analysis.

Experimental

Crystal Data A rectangular prismatic crystal with approximate dimensions 0.15 x 0.21 x 0.25 mm was selected and mounted inside a 0.30 mm thin-walled Lindeman glass capillary and subsequently attached to a standard goniometer head. From three preliminary ω-oscillation photographs taken on an automated four-circle x-ray diffractometer at various χ and ϕ settings, seven independent reflections were selected and their coordinates were input to an automatic indexing algorithm.[3]

The resulting reduced cell and reduced cell scalars

indicated monoclinic symmetry. Observed layer line spacings were within experimental error of those predicted for this cell. The least-squares refinement of the lattice constants[4] based on precise $\pm 2\theta$ measurements of 15 strong independent reflections, using Mo K_α radiation, λ = 0.70954 Å, at 27°C, yielded $\underline{a}$ = 6.574(2) Å, $\underline{b}$ = 9.354(2) Å, $\underline{c}$ = 9.885(2) Å, and β = 107.4(2)°.

Collection and Reduction of X-Ray Intensity Data

Data were collected at room temperature on an automated four-circle diffractometer designed and built in this laboratory.[5] The diffractometer is interfaced to a PDP-15 computer in a time-sharing mode and is equipped with a scintillation counter. Graphite-monochromated Mo K_α radiation was used for data collection.

All data (953 reflections) within a 2θ sphere of 45° were measured in the hkl and hk$\bar{l}$ octants using an ω-scan data collection technique.

As a general check on electronic and crystal stability, the intensities of three standard reflections were remeasured every 75 reflections. These standard reflections were not observed to vary significantly throughout the entire data collection period. Examination of the data revealed systematic absences for 0k0 when k = 2n+1 and a Howells, Phillips and Rogers test[6] indicated acentric symmetry; hence the space group was determined to be $P2_1$.

The intensity data were corrected for Lorentz-polarization effects. Since $\mu = 6.41$ cm^{-1} and minimum and maximum transmission factors differed by less than 5%, no absorption corrections were made. The estimated variance in each intensity was calculated by

$$\sigma_I^2 = C_T + k_t C_B + (0.03C_T)^2 + (0.03C_B)^2$$

where C_T, k_t and C_B represent the total count, a counting time factor and the background count, respectively; the factor 0.03 represents an estimate of nonstatistical errors. The estimated standard deviations in the structure factors were calculated by the finite-difference method.[7] Equivalent zone data were averaged and 737 reflections for which $F_o > 3\sigma(F)$ were retained for structural refinement.

Solution and Refinement

The position of one sulfur atom was obtained by analysis of a sharpened three-dimensional Patterson function. The remaining atoms were found by successive structure factor[8] and electron density map[9] calculations. These atomic positions were subsequently refined by a full-matrix least-squares procedure[8] minimizing the function $\Sigma\omega(|F_o|-|F_c|)^2$ where $\omega = 1/\sigma_F^2$, to a conventional residual index of $R = \Sigma||F_o|-|F_c||/\Sigma|F_o| = 0.069$. At this stage all 12 nonhydrogen atoms had been refined with anisotropic thermal parameters. The scattering factors used were those of Hanson et al.,[10]

modified for the real and imaginary parts of anomalous dispersion.[11] The scattering factor for hydrogen was that of Stewart et al.[12]

The hydrogen positions were then calculated using bond lengths of 1.0 Å. The isotropic hydrogen temperature factors were set equal to 4.0 Å^2. Further refinement cycles without varying the hydrogen parameters did not significantly alter any atomic parameters and the residual index converged to $R = 0.068$.

The final positional and thermal parameters are listed in Tables 1 and 2, respectively. Standard deviations were calculated from the inverse matrix of the final least-squares cycle. Bond distances and angles[13] are listed in Table 3.

Description and Discussion

A view of the dimethoate molecule depicting 50% probability ellipsoids[14] is provided in Figure 1, and a stereographic view of the unit cell is provided in Figure 2. As was found for all previously studied organophosphorus insecticides, the geometry around the phosphorus can be described as a distorted tetrahedron and within experimental error is identical to that found for amidithion. The angles including the doubly bonded sulfur and the methoxy oxygens are about 9° greater than the tetrahedral angle while the O1-P-O2 angle is 94.7°.

Table 1. Final atomic positional parameters[1] for dimethoate

Atom	x	y	z
S1	0.3636(7)[2]	0.1397(0)	0.1037(5)
S2	-0.0399(4)	0.2210(7)	0.2089(3)
P	0.2804(5)	0.2508(7)	0.2384(3)
O1	0.402(1)	0.229(1)	0.3996(7)
O2	0.323(1)	0.419(1)	0.2406(9)
O3	-0.041(2)	0.145(1)	0.510(1)
N	0.065(2)	0.366(1)	0.593(1)
C1	0.444(2)	0.085(2)	0.458(2)
C2	0.250(3)	0.504(2)	0.114(2)
C3	-0.087(2)	0.339(1)	0.344(1)
C4	-0.015(2)	0.273(1)	0.491(1)
C5	0.133(3)	0.321(2)	0.743(2)
NH	0.0837	0.4685	0.5678
C3H1	0.017	0.423	0.350
C3H2	0.767	0.380	0.333
C1H1	0.3082	0.0442	0.4704
C1H2	0.5558	0.0871	0.5508
C1H3	0.4898	0.0223	0.3901
C2H1	0.3129	0.6027	0.1344
C2H2	0.0919	0.5106	0.0847
C2H3	0.2983	0.4594	0.0376
C5H1	0.0047	0.3109	0.7770
C5H2	0.2329	0.3923	0.8024
C5H3	0.2067	0.2254	0.7516

[1]Positional parameters are given in fractional unit cell coordinates.

[2]In this and succeeding tables, estimated standard deviations are given in parentheses for the least significant figures. Since hydrogen parameters were not refined, no standard deviations are given.

Table 2. Final atomic thermal parameters[1] for dimethoate

Atom	β_{11}	β_{22}	β_{33}	β_{12}	β_{13}	β_{23}
S1	485(15)	275(9)	228(7)	62(10)	140(8)	-50(6)
S2	286(9)	151(5)	156(4)	-14(6)	41(5)	-36(4)
P	280(8)	168(6)	131(4)	7(6)	45(4)	-7(4)
O1	358(24)	187(14)	140(10)	10(19)	15(12)	27(12)
O2	435(30)	161(14)	155(12)	-64(16)	47(15)	22(11)
O3	518(36)	91(13)	201(14)	-6(16)	93(17)	4(11)
N1	557(41)	79(13)	145(14)	6(19)	58(19)	11(12)
C1	452(56)	218(28)	323(36)	61(31)	59(35)	148(28)
C2	728(67)	162(23)	180(22)	-55(35)	34(31)	78(19)
C3	328(36)	96(13)	155(15)	25(20)	96(19)	-16(14)
C4	407(38)	81(16)	146(16)	0(20)	104(20)	26(14)
C5	1224(109)	148(23)	162(21)	21(40)	17(38)	4(20)

[1]In this and succeeding tables the β_{ij}'s are x10^4 and are defined by $\exp[-(\beta_{11}h^2 + \beta_{22}k^2 + \beta_{33}l^2 + 2\beta_{12}hk + 2\beta_{13}hl + 2\beta_{23}kl)]$. The hydrogen atoms were included with fixed isotropic thermal parameters $B_H = 4.0$.

Table 3. Bond distances (Å) and angles (°) for dimethoate

		Distances	
P-S1	1.895(5)	S2-C3	1.83(1)
P-S2	2.056(4)	C3-C4	1.52(2)
P-O1	1.568(8)	C4-O3	1.23(1)
P-O2	1.597(9)	C4-N	1.32(1)
O1-C1	1.46(2)	N-C5	1.47(2)
O2-C2	1.44(2)		
		Angles	
S1-P-O1	118.4(4)	P-O2-C2	121.6(8)
S1-P-O2	117.6(4)	P-S2-C3	101.9(4)
S1-P-S2	109.0(2)	S2-C3-C4	112.4(9)
O1-P-O2	94.7(5)	C3-C4-O3	122(1)
O1-P-S2	108.4(4)	C3-C4-N	114(1)
O2-P-S2	107.6(4)	C4-N-C5	121(1)
P-O1-C1	120.3(9)	O3-C4-N	125(1)

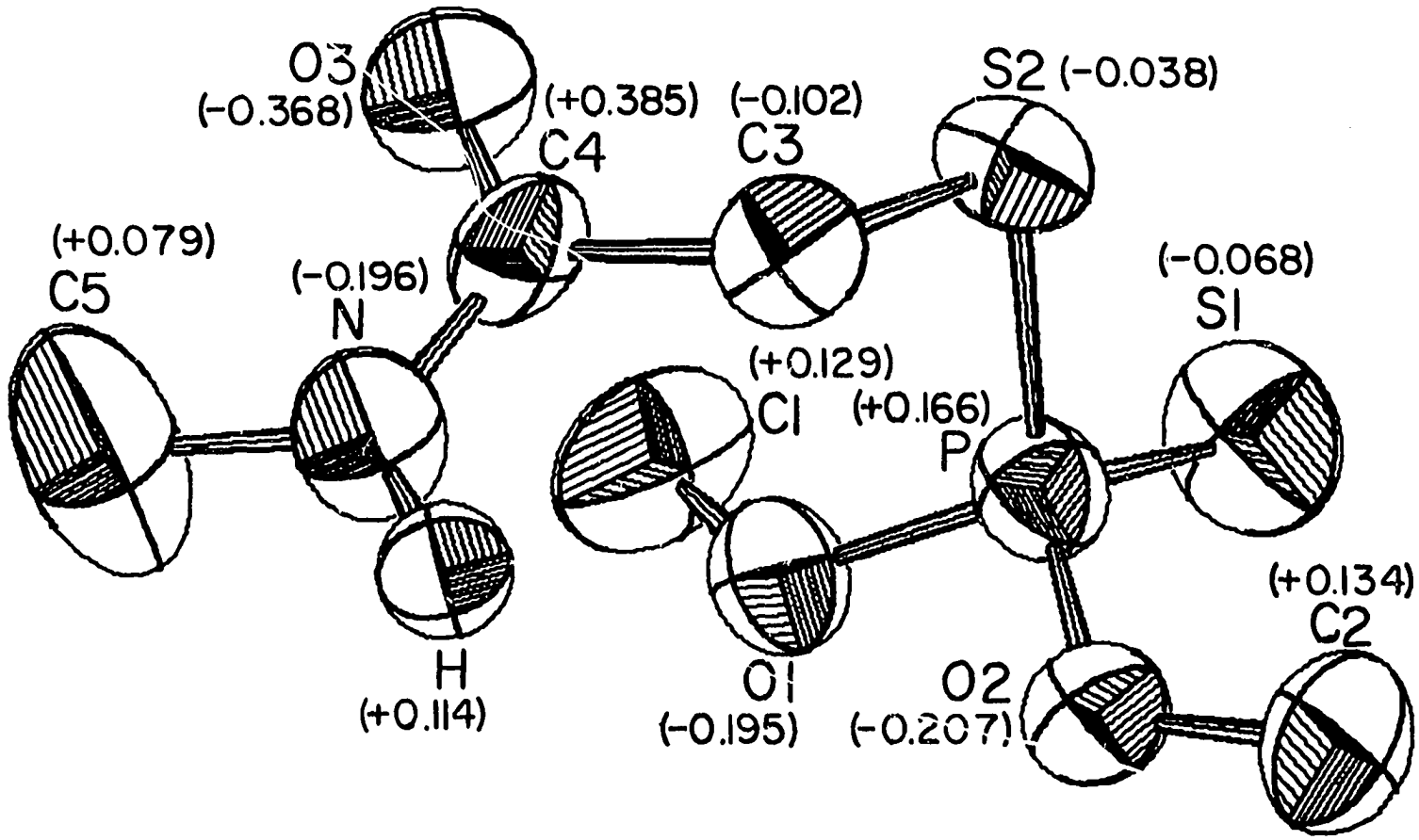

Figure 1. View of the dimethoate molecule with methyl and ethyl hydrogens omitted. Charge densities are from CNDO/2 molecular orbital calculations and ellipsoids are at 50% probability level.

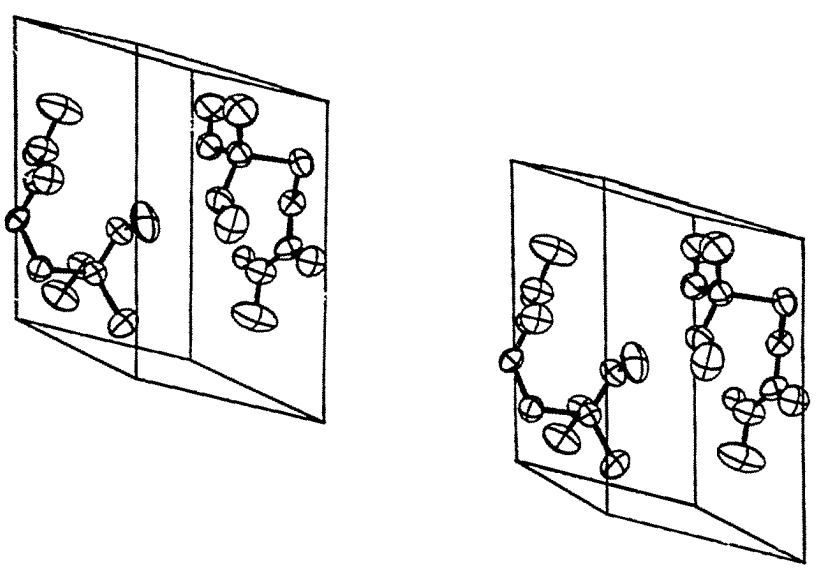

Figure 2. Unit cell stereograph of dimethoate.

CNDO/2 molecular orbital calculations[15] were carried out to compute approximate values for the charge density distribution in dimethoate; the results are shown in Figure 1. The AChE model of Krupka[16] requires two regions of a net δ(+) charge to bind to the reactive site of AChE. Chothia and Pauling[17] reported that when acetylcholine is in a proper configuration to react with bovine erythrocyte AChE, the nitrogen to carbonyl carbon distance is about 4.7 Å. Hollingworth et al.,[18] however, concluded that the corresponding distance in fly head AChE may be as much as 1 Å longer than in the mammalian enzyme. O'Brien[19] has reported a range of 4.5-5.9 Å for insect AChE. With these distances in mind the notable centers of positive charge in dimethoate are on atoms C4, H and C5 which are respectively 3.60, 4.35 and 5.40 Å from the phosphorus. The relatively small charge on C5 makes it an unlikely site for binding. The PC4 distance is significantly shorter and the P-H distance longer than the corresponding distances in amidithion[2] (3.91 and 4.24 Å, respectively). By contrast, the primary positive center separation distance in azinphos-methyl[1] is 4.83 Å. The site separation for dimethoate would appear to be too short for efficient binding to the enzyme. On the basis of solid state configurations one would expect the toxicity of dimethoate in mammalian systems to be similar to that of amidithion and much less than that of azinphos-methyl. A comparison of acute

oral LD_{50}'s for rats confirms this trend: over 600 mg/kg for dimethoate,[20] 600-660 for amidithion[2] and 15 for azinphos-methyl.[1] However, this distance argument would also suggest that dimethoate would be significantly less effective in insect systems unless enzyme interactions with C5 are greater than we have assumed. It is generally accepted that the oxidized phosphate form is responsible for enzyme inhibition. Such oxidation, however, would most likely enhance the charge on the phosphorus and cause only minor perturbations on the rest of the molecular configuration.

An examination of intramolecular interactions indicates that the in vivo configuration could be quite different from the solid state configuration. By allowing free rotation about the S2-C3 bond the positive center separations could be increased to approximately 4.5 Å for P-C4 and 5.4 Å for P-H. In dimethoate, as in amidithion, delocalization effects cause the C3, C4, O3, N and C5 atoms to be nearly coplanar, the greatest deviation from the least-squares plane defined by these five atoms being 0.02 Å. However, in the solid state configuration the angle between the normal to this plane and the P=S bond is 50.47°. In a series of OP's studied in this Laboratory[21-27] in which intramolecular interactions tend to restrict the range of possible molecular configurations, the angle between the P=X (X = S or O) bond and the normal to the planar portion of the molecule is usually in the range of

20°-40°. If the angle between the P=S bond and the planar moiety is an important topographical factor in the binding of the insecticide to the enzyme, then some rotation to modify this angle and at the same time increase the positive site separations may be expected. Hence, for dimethoate, the most favorable configuration for interaction with the enzyme is most likely not the same as the solid state configuration.

THE CRYSTAL AND MOLECULAR STRUCTURE OF ISOPROPYL-O-METHYL-O-(3,5,6-TRICHLORO-2-PYRIDYL) PHOSPHORAMIDOTHIOATE

Introduction

Ronnel,[21] bromophos,[22] ronnel oxon[23] and crufomate[24] are all phenoxy OP's which have been studied in this laboratory. The study of heteronuclear ring systems such as fospirate,[25] chlorpyrifos[26] and Dowco 214[27] was begun in order to note any conformational similarities and/or dissimilarities resulting from the replacement of one or more ring carbon atoms with nitrogen. Continuing with the latter series we carried out a crystal structure analysis of isopropyl-O-methyl-O-(3,5,6-trichloro-2-pyridyl) phosphoramidothioate, hereafter referred to as IPAT, an amido homolog of Dowco 214. Although this compound was never commercially produced it has been shown to have good insecticidal properties[28].

Experimental

Crystal Data A rectangular prismatic crystal with approximate dimensions 0.40 x 0.44 x 0.30 mm was selected and mounted on the end of a glass fiber with Elmer's Glue-All and subsequently attached to a standard goniometer head. From three preliminary ω-oscillation photographs taken on an automated four-circle x-ray diffractometer at various χ and ϕ

settings, 10 independent reflections were selected and their coordinates were input to an automatic indexing algorithm.[3]

The resulting reduced cell and reduced cell scalars indicated triclinic symmetry. Observed layer line spacings were within experimental error of those predicted for this cell. The least-squares refinement of the lattice constants[4] based on precise $\pm 2\theta$ measurements of 15 strong independent reflections, using Mo K_α radiation, λ = 0.70954 Å, at 27°C, yielded $\underline{a}$ = 10.319(5) Å, $\underline{b}$ = 10.730(6) Å, $\underline{c}$ = 8.449(4) Å, α = 99.01(2)°, β = 114.02(1)° and γ = 62.64(1)°.

Collection and Reduction of X-Ray Intensity Data

Data were collected at room temperature on an automated four-circle diffractometer designed and built in this laboratory.[5] The diffractometer is interfaced to a PDP-15 computer in a time-sharing mode and is equipped with a scintillation counter. Graphite-monochromated Mo K_α radiation was used for data collection.

All data (2812 reflections) within a 2θ sphere of 50° were measured in the hkl, $hk\bar{l}$, $h\bar{k}l$ and $h\bar{k}\bar{l}$ octants using an ω-scan data collection technique.

As a general check on electronic and crystal stability, the intensities of six standard reflections were remeasured every 75 reflections. These standard reflections were not observed to vary throughout the entire data collection period.

The intensity data were corrected for Lorentz-polarization effects and, since $\mu = 8.17\ cm^{-1}$, absorption corrections were not made; minimum and maximum transmission factors were 0.735±0.045. The estimated variance in each intensity was calculated by

$$\sigma_I^2 = C_T + k_t C_B + (0.03C_T)^2 + (0.03C_B)^2$$

where C_T, k_t and C_B represent the total count, a counting time factor and background count, respectively, and the factor 0.03 represents an estimate of nonstatistical errors. The estimated standard deviations in the structure factors were calculated by the finite-difference method.[7] Equivalent zone data were averaged and 2173 reflections for which $F_o > 3\sigma(F)$ were retained for structural refinement.

Solution and Refinement

A Howells, Phillips and Rogers test[6] indicated centric symmetry and the space group $P\bar{1}$ was assumed. After numerous unsuccessful attempts to solve this structure using MULTAN[29] and Patterson superposition techniques, the structure was finally determined using a direct method program written in this laboratory[30] and utilizing a symbolic addition approach.[31] Using the 300 reflections with $|E| > 1.5$, 14 nonhydrogen atoms were located on the resulting E-map. The positions of the remaining nonhydrogen atoms were determined by successive structure factor[8] and electron-density map[9]

calculations. These atomic positions were subsequently refined by a full-matrix least-squares procedure,[8] minimizing the function $\Sigma\omega(|F_o|-|F_c|)^2$ where $\omega = 1/\sigma_F^2$. This refinement yielded a conventional residual index of $R = \Sigma||F_o|-|F_c||/\Sigma|F_o| = 0.074$. At this stage all 18 nonhydrogen atoms had been refined using anisotropic thermal parameters. The scattering factors used were those of Hanson et al.,[10] modified for the real and imaginary parts of anomalous dispersion.[11] The scattering factor for hydrogen was that of Stewart et al.[12]

The aromatic hydrogen position was calculated at 0.95 Å from the corresponding carbon atom [C3] and hydrogens were placed 1.0 Å from N2 and C6 assuming tetrahedral geometry. Methyl hydrogens were inserted in approximately tetrahedral positions using the precise positions of the methyl carbons and the attached atoms. Each set of methyl hydrogens was rotated by 60° about the A-Me bond (A = C or O) and each methyl hydrogen was assigned half-occupancy. As a result a "doughnut" of hydrogens was approximated. The methyl C-H distances were set equal to 1.0 Å and all isotropic hydrogen temperature factors were set equal to 4.5 Å^2.

Subsequent anisotropic least-squares refinement without varying the hydrogen parameters converged to R = 0.058. Since the nonhydrogen atom parameters shifted slightly, all of the hydrogen positions were recalculated. Further refine-

ment cycles did not significantly alter any atomic parameters and the residual index did not change.

The final positional and thermal parameters are listed in Tables 4 and 5, respectively. Standard deviations were calculated from the inverse matrix of the final least-squares cycle. Bond lengths and angles[13] are listed in Tables 6 and 7, respectively.

Description and Discussion

A perspective drawing of IPAT depicting 50% probability ellipsoids[14] is provided in Figure 3. As expected, the pyridoxyl group is essentially planar, the greatest deviation from the least-squares plane defined by the six-membered ring, the three attached chlorines and O1 being 0.042 Å for O1, in good agreement with the results from previous pyridoxy OP structure determinations.[25-27] The crystal packing may be regarded as primarily van der Waals in nature as all intermolecular distances are larger than or on the order of the sum of the van der Waals radii. Consequently, the molecular configuration is not likely to be a result of crystal packing.

As has been found in previous studies of OP insecticides, the O1-C1 distance is significantly shorter than the O2-C9 distance while the P-O1 bond is longer than the P-O2 bond. This is consistent with the overlap of a p_z orbital on

Table 4. Final atomic positional parameters

Atom	x	y	z
Cl1	0.6195(2)	0.3810(1)	-0.2675(2)
Cl2	0.7011(2)	0.7296(1)	0.2577(2)
Cl3	0.8302(2)	0.4756(1)	0.5173(2)
S	0.6139(1)	0.1145(1)	0.2451(1)
P	0.7517(1)	0.0589(1)	0.1217(1)
O1	0.7342(4)	0.1831(3)	0.0144(4)
O2	0.9345(3)	0.0006(3)	0.2328(4)
N1	0.7783(4)	0.3298(3)	0.2421(5)
N2	0.7265(4)	-0.0530(3)	-0.0250(4)
C1	0.7311(5)	0.3103(4)	0.0751(6)
C2	0.6772(5)	0.4134(4)	-0.0493(6)
C3	0.6687(5)	0.5441(4)	0.0069(6)
C4	0.7155(5)	0.5659(4)	0.1843(7)
C5	0.7720(5)	0.4553(4)	0.2977(6)
C6	0.8211(6)	-0.1188(6)	-0.1340(6)
C7	0.8732(7)	-0.2758(6)	-0.1354(8)
C8	0.7276(8)	-0.0503(8)	-0.3167(7)
C9	0.0137(6)	-0.1259(5)	0.3419(7)
N2H1	0.7378	-0.1323	0.0357
C3H1	0.6301	0.6174	-0.0736
C6H1	0.9159	-0.0999	-0.0862
C7H1	0.7871	-0.2952	-0.1356
C7H2	0.8729	-0.3066	-0.0298
C7H3	0.9704	-0.3217	-0.0298
C7H4	0.9822	-0.3255	-0.1356
C7H5	0.8964	-0.3141	-0.2415
C7H6	0.7989	-0.2990	-0.2415
C8H1	0.7980	-0.0344	-0.3565
C8H2	0.7284	0.0427	-0.3152
C8H3	0.6376	0.0416	-0.3152
C8H4	0.6162	-0.0365	-0.3565
C8H5	0.6856	-0.1136	-0.3978
C8H6	0.7767	-0.1126	-0.3978
C9H1	0.9343	-0.1397	0.3669
C9H2	0.9967	-0.1009	0.4533
C9H3	1.0942	-0.1161	0.4533
C9H4	1.1293	-0.1700	0.3669
C9H5	1.0669	-0.2087	0.2806
C9H6	0.9694	-0.1936	0.2806

Table 5. Final atomic thermal parameters[1]

Atom	β_{11}	β_{22}	β_{33}	β_{12}	β_{13}	β_{23}
Cl1	222(2)	160(2)	224(3)	-58(2)	104(2)	36(2)
C12	255(3)	99(1)	384(4)	-87(2)	93(3)	4(2)
C13	281(3)	139(2)	238(3)	-110(2)	76(2)	-16(2)
S	145(2)	114(1)	178(2)	-59(1)	68(1)	-7(1)
P	125(2)	86(1)	151(2)	-50(1)	45(1)	7(1)
O1	205(5)	106(4)	193(6)	-78(4)	82(4)	8(3)
O2	127(4)	116(4)	191(6)	-60(3)	38(4)	5(4)
N	165(6)	99(4)	211(8)	-65(4)	79(5)	3(4)
N2	154(6)	108(4)	171(6)	-62(4)	68(5)	-14(4)
C1	138(6)	92(5)	222(9)	-50(5)	79(6)	10(5)
C2	133(6)	114(5)	222(9)	-44(5)	78(6)	31(5)
C3	146(7)	98(5)	284(1)	-43(5)	90(7)	45(6)
C4	145(7)	84(5)	302(12)	-44(5)	82(7)	11(6)
C5	155(7)	108(5)	243(10)	-63(5)	76(7)	-1(6)
C6	188(8)	187(7)	225(10)	-121(7)	114(8)	-72(7)
C7	242(11)	204(9)	367(16)	-111(8)	191(11)	-127(10)
C8	347(15)	340(14)	197(11)	-207(12)	122(11)	-30(10)
C9	173(8)	115(6)	237(10)	-44(6)	33(7)	30(6)

[1]The hydrogen atoms were included with fixed isotropic thermal parameters $B_H = 4.5$.

Table 6. Bond distances (Å) for IPAT

P-S	1.923(1)
P-O1	1.628(3)
P-O2	1.578(3)
P-N2	1.613(3)
O2-C9	1.454(5)
N2-C6	1.481(5)
C6-C7	1.514(7)
C6-C8	1.532(8)
O1-C1	1.372(5)
C1-C2	1.399(5)
C2-C3	1.383(6)
C3-C4	1.393(6)
C4-C5	1.390(6)
C5-N1	1.336(5)
N1-C1	1.309(5)
C2-Cl1	1.724(5)
C4-Cl2	1.728(4)
C5-Cl3	1.714(5)

Table 7. Bond angles (°)

S-P-O1	116.4(1)	C3-C4-C5	119.0(4)
S-P-O2	117.3(1)	C4-C5-N1	122.2(4)
S-P-N2	113.2(1)	C5-N1-C1	118.7(4)
O1-P-O2	97.6(1)	C11-C2-C1	121.5(3)
O1-P-N2	102.9(2)	C11-C2-C3	120.3(3)
O2-P-N2	107.4(2)	C12-C4-C3	119.3(3)
P-O2-C9	119.0(3)	C12-C4-C5	121.8(4)
P-N2-C6	124.9(3)	C13-C5-C4	121.3(3)
P-O1-C1	126.9(3)	C13-C5-N1	116.4(3)
O1-C1-C2	116.7(4)	N2-C6-C7	109.7(4)
O1-C1-N1	119.8(3)	N2-C6-C8	110.4(4)
C1-C2-C3	118.3(4)	C7-C6-C8	112.4(5)
C2-C3-C4	118.3(4)	N1-C1-C2	123.4(4)

Table 8. Torsional Angles (°)

P-O1-C1-C2	-164.9	S-P-O2-C9	61.2
P-O1-C1-N1	15.6	S-P-N2-C6	-177.0
C1-O1-P-S	49.1	O1-P-O2-C9	-173.7
C1-O1-P-N2	173.5	O1-P-N2-C6	56.4
C1-O1-P-O2	-76.6		

Figure 3. View of IPAT with partial charge densities obtained from CNDO/2 molecular orbital calculations. The thermal ellipsoids are drawn at the 50% probability level.

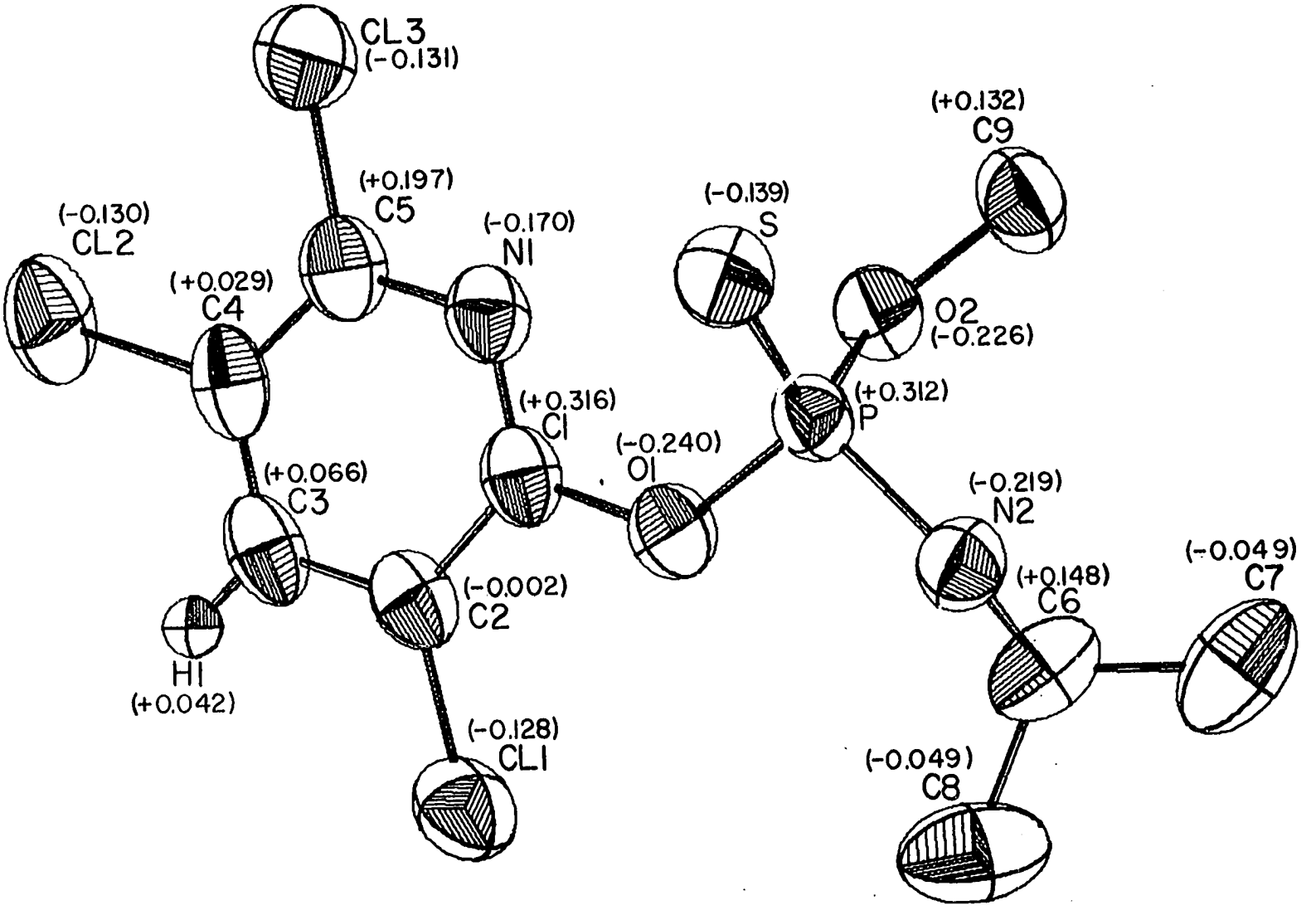
CL3
(-0.131)
(+0.197)
C5
(-0.130)
CL2
(+0.029)
C4
(-0.170)
N1
(-0.139)
S
(+0.132)
C9
O2
(-0.226)
(+0.316)
C1
(+0.312)
P
(-0.240)
O1
(+0.066)
C3
(-0.219)
N2
(-0.049)
C7
(+0.148)
C6
(-0.002)
C2
H1
(+0.042)
(-0.128)
CL1
(-0.049)
C8

O1 with the ring system leading to a weakening of the P-O1 bond, an effect which should enhance phosphorylation.[32] In addition, the P-O1 bond in IPAT is longer than in any other OP studied thus far; this is apparently a result of replacing an oxygen with nitrogen in the phosphate group. IPAT, like the other pyridoxy OP insecticides chlorpyrifos,[26] fospirate,[25] and Dowco 214,[27] has a C1-O1 bond length about 4σ shorter than the corresponding bond in the phenoxy insecticides; this appears to be a result of the replacement of a ring carbon by the more electronegative nitrogen. The geometry about the phosphorus atom is distorted tetrahedral such that the S=P-X (X= O or N) angles are all greater than the tetrahedral angle of 109.47° while the O-P-O and O-P-N angles are all less than 109°.

The internal ring angles are identical to their counterparts in the pyridoxy insecticides. Those angles with nitrogen as a terminal atom are greater than 120° while the other angles are all less than 120°. The angle between the normal to the ring and the P=S vector is 33.4°, well-within the range of 20°-40° observed for most of the OP's studied.

The phosphorus and Cl1 atoms lie on opposite sides of a plane perpendicular to the ring and containing the O1-C1 bond. The position of the phosphorus is apparently influenced by several intramolecular interactions. The N1-S and N1-O2 distances are 3.45 and 3.14 Å, respectively, while the

sums of the respective van der Waals radii are 3.35 and 2.9 Å,[33] and the Cl1-C8 distance of 4.2 Å is 0.4 Å greater than the sum of their van der Waals radii. The absence of a substituent on N1 allows the phosphate group to avoid Cl1. Due to the π-character of the O1-C1 bond, suggested above, one would expect the phosphorus atom to lie in the plane of the aromatic group and indeed it is only 0.4 Å away from the least-squares plane defined by the ring and the four atoms attached to it. The resulting N1-C1-O1-P torsional angle of 15.6° (cf. Table 8) is in the range of 10°-30° observed for the other pyridoxy OP's; the corresponding angle in the phenoxy OP's is in the range of 50°-80°.

In considering autotoxicosis through inhibition of AChE by organophosphorus insecticides, it is useful to recall that the nitrogen to carbonyl-carbon distance in acetylcholine is estimated at 4.7 Å when the molecule is in a proper configuration to react with bovine erythrocyte AChE.[17] The distance between anionic and esteratic sites of fly head AChE, however, may be as much as 1 Å longer than in the mammalian enzyme.[18] O'Brien[19] has reported a range of 4.5-5.9 Å for the insect AChE. A comparison of some intramolecular distances with these values should give some insight into the toxicity/activity of any insecticide. In addition to appropriate site separations, the two atoms involved must both have a net δ(+) charge to be in agreement with the AChE model

of Krupka.[16]

CNDO/2 molecular orbital calculations[15] were carried out to compute approximate values for the charge density distribution in IPAT; the results are shown in Figure 3. Examination of this figure shows that there are four possible positive sites that could be involved in enzyme binding. They are C3, C4, C5 and H1, and the corresponding distances from the phosphorus are, respectively, 5.06, 5.24, 4.35, and 5.89 Å. It is interesting to note that these distances are all greater than the corresponding distances in the other pyridoxy OP's. With a charge of only 0.029e, C4 is probably not a major contributor to inhibition. C3 and H1 lie within the range of distances appropriate for insect AChE and are slightly longer than the mammalian distance. The C5 distance is too short for insect AChE but could be an important factor in reactions with mammalian AChE.

An examination of intramolecular interactions indicates that rotation about the P-O1 and O1-C1 bonds could occur in vivo. Rotation about the P-O1 bond would have no effect on the positive charge center separations but rotation about the O1-C1 bond to a P-O1-C1-N1 torsional angle of about 90°, similar to the solid state configuration of the phenoxy OP's, would decrease the P-C3 distance, for example, by about 0.25 Å bringing it into a range suitable for interaction with mammalian AChE. Such a rotation would change the position of

the phosphorus relative to other ring substituents and this could be an important factor due to steric influences of the insecticide on the AChE molecule.

THE CRYSTAL AND MOLECULAR STRUCTURE OF LEPTOPHOS

Introduction

Several previously reported crystal structure analyses have discussed the relationship between structure and toxicity/activity of insecticides. The establishment of such a relationship is of even greater importance when the insecticide is a chiral molecule. The stereospecificity of AChE inhibition reactions with asymmetric organophosphorus compounds was first suggested by Michel in 1955[34] but very little work has been done since that time. Since Aaron et al.,[35] first succeeded in demonstrating that the levo-isomer of the ethylphosphonate analog of demeton-S reacted 10 to 20 times faster with cholinesterases than the dextro-isomer, only a few enantiomers of biologically active organophosphorus compounds have been isolated and studied.[36-39] Interestingly, the results of these studies have shown that the AChE molecule is highly stereospecific of asymmetric organophosphorus inhibitors, although its natural substrate, acetylcholine, has no asymmetric center.

Recently, Fukuto and Allahyari began a toxicological study of some chiral insecticides including leptophos[40] (O-methyl-O-(4-bromo-2,5-dichlorophenyl) phenylphosphonothioate.) In order to resolve the enantiomers the O-methyl

phenylphosphonothioic acid was synthesized according to the following sequence of reactions:

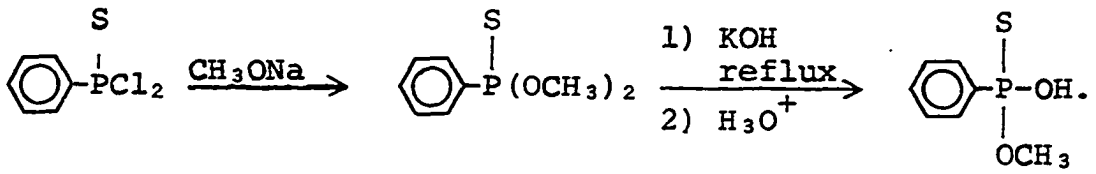

1

The acid was purified by recrystallization as the dicyclohexylamine salt. After purification, the racemic 1 was treated with (-)-α-phenylethylamine which, after four recrystallizations from ethyl acetate-hexane resulted in the separation of (+)- and (-)-1 as the α-phenylethylammonium salt

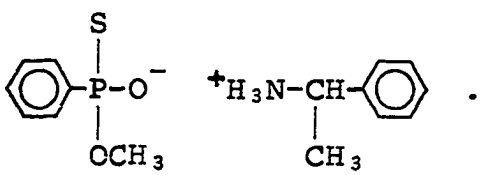

The synthesis of (-)-leptophos then followed the sequence of reactions:

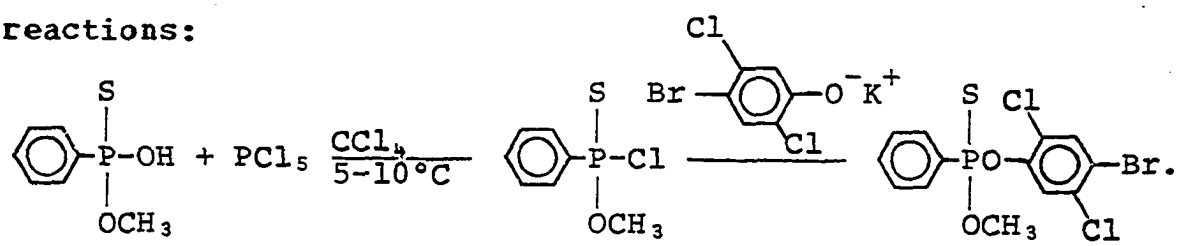

(+)-1 (+)-chloridate (-)-leptophos

Since the absolute configuration around the phosphorus atom was unknown, they kindly provided us with crystals for structural analysis. These crystals, however, were found to contain a racemic mixture of the two enantiomers due to a tendency for the chloridate to racemize. Although the

required configurational information was not available from these crystals, the structural analysis was completed to add to our library of molecular parameters for insecticides.

Upon learning of the problem with the first sample, Allahyari then supplied crystals of the (-)-α-phenylethylammonium salt. Since the absolute configuration around the asymmetric carbon was already known,[41] the correct configuration around the phosphorus in the salt, and hence in leptophos, could be deduced.

Experimental

Crystal Data A prismatic crystal with approximate dimensions 0.16 x 0.22 x 0.30 mm was selected and mounted on the end of a glass fiber with Elmer's Glue-All and subsequently attached to a standard goniometer head. From three preliminary ω-oscillation photographs taken on an automated four-circle x-ray diffractometer at various χ and ϕ settings, 10 independent reflections were selected and their coordinates were input to an automatic indexing algorithm.[3]

The resulting reduced cell and reduced cell scalars indicated monoclinic symmetry. This was confirmed by taking oscillation photographs about each axis; only the b-axis displayed mirror symmetry. Observed layer line spacings were within experimental error of those predicted for this cell. The least squares refinement of the lattice constants[4] based

on the precise ±2θ measurements of 9 strong independent reflections, using Mo Kα radiation, λ = 0.70954 Å, at 27°C, yielded $\underline{a}$ = 12.394(4), $\underline{b}$ = 7.642(2), $\underline{c}$ = 16.543(4) Å, and β = 97.45(6)°.

Collection and Reduction of X-Ray Intensity Data

Data were collected at room temperature on an automated four-circle diffractometer designed and built in this laboratory.[5] The diffractometer is interfaced to a PDP-15 minicomputer in a time-sharing mode and is equipped with a scintillation counter. Graphite-monochromated Mo Kα radiation was used for data collection.

All data (6385 reflections) within a 2θ sphere of 50° were measured in the hkl, hkl̄, hk̄l and hk̄l̄ octants using an ω-scan data collection technique.

As a general check on electronic and crystal stability, the intensities of six standard reflections were remeasured every 75 reflections. These standard reflections were not observed to vary throughout the entire data collection period.

The intensity data were corrected for Lorentz-polarization effects and for absorption; minimum and maximum transmission factors were 0.52 and 0.62 respectively, with μ = 33.80 cm^{-1}. The estimated variance in each intensity was calculated by:

$$\sigma_I^2 = [C_T + k_t^2 C_B + (0.03C_T)^2 + (0.03C_B)^2 + (0.03C_N)^2]/A^2$$

where C_B, C_T and C_N represent background, total and net counts, respectively, k_t is a counting time factor and A is a transmission factor; the factor 0.03 represents an estimate of nonstatistical errors. The estimated deviations in the structure factors were calculated by the finite difference method.[7] Equivalent data were averaged and 2331 reflections for which $F_o > 3.0\sigma(F)$ were retained for structural refinement.

Solution and Refinement

A statistical test of the data[6] indicated centric symmetry and the observed extinction conditions 0k0: k=2n+1, and h0l: h=2n+1 determined the space group to be $P_{2_1/a}$. After conventional Patterson and direct method procedures failed to yield a solution, the structure was found via the new Patterson superposition method of Jacobson and Beckman.[42] This method located all the nonhydrogen atoms except for those in the phenyl ring. The remaining atomic positions were determined by successive structure factor[43] and electron-density map[9] calculations. These atomic positions were subsequently refined by a block-diagonal least-squares procedure,[43] minimizing the function $\Sigma\omega(|F_o| - |F_c|)^2$ where $\omega = 1/\sigma_F{}^2$. This refinement yielded a conventional residual index of $R = \Sigma||F_o| - |F_c||/\Sigma|F_o| = 0.059$. At this stage all 20 nonhydrogen atoms had been refined using anisotropic thermal

parameters. The scattering factors used were those of Hanson et al.,[10] modified for the real and imaginary parts of anomalous dispersion.[11] The scattering factor for hydrogen was that of Stewart et al.[12]

Positions for the hydrogen atoms were calculated using a bond distance of 0.95 Å for the aromatic hydrogens and 1.00 Å for the methyl hydrogens. Subsequent full-matrix refinement, without varying the hydrogen parameters, converged to $R = 0.051$.

The final positional and thermal parameters are listed in Tables 9 and 10, respectively. Standard deviations were calculated from the inverse matrix of the final least-squares cycle. Bond distances and angles[13] are listed in Tables 11 and 12, respectively.

Description and Discussion

A computer drawing[14] of the leptophos molecule is provided in Figure 4 and a stereographic view of the contents of one unit cell is shown in Figure 5. As expected, the phenoxy and phenyl groups are both essentially planar, (cf. Table 13).

As has been found in all the other OP's, the geometry about the phosphorus can be described as distorted tetrahedral. All angles of the type S=P-X (X = C or O) are greater than the tetrahedral angle of 109.47° while the other angles

Table 9. Final atomic positional parameters for leptophos

Atom	x	y	z
Br	0.17314(4)	0.43239(7)	0.40610(3)
Cl1	0.9707(1)	0.2163(2)	0.46684(7)
Cl2	0.3424(1)	0.4733(2)	0.72818(8)
S	0.3313(1)	0.0127(2)	0.79420(8)
P	0.18592(9)	0.0863(2)	0.80300(7)
O1	0.1471(2)	0.2699(4)	0.7605(2)
O2	0.0944(3)	0.9609(4)	0.7604(2)
C1	0.1541(3)	0.2999(6)	0.6782(3)
C2	0.2400(3)	0.3974(6)	0.6558(3)
C3	0.2448(4)	0.4351(6)	0.5747(3)
C4	0.1638(4)	0.3776(6)	0.5157(3)
C5	0.0752(3)	0.2837(5)	0.5384(3)
C6	0.0718(3)	0.2456(6)	0.6201(3)
C7	0.1532(4)	0.1251(6)	0.9031(3)
C8	0.2166(4)	0.0499(6)	0.9706(3)
C9	0.1866(5)	0.0691(7)	0.0469(3)
C10	0.0967(5)	0.1607(8)	0.0591(3)
C11	0.0343(4)	0.2384(7)	0.9942(4)
C12	0.0606(4)	0.2194(7)	0.9157(3)
C13	0.1047(5)	0.7759(8)	0.7606(4)
C3H	0.3042	0.5001	0.5592
C6H	0.0124	0.1806	0.6356
C8H	0.2796	0.9851	0.9621
C9H	0.2297	0.0172	0.0922
C10H	0.0774	0.1737	0.1124
C11H	0.9713	0.3032	0.0027
C12H	0.0175	0.2714	0.8704
C13H1	0.1744	0.7419	0.7401
C13H2	0.1052	0.7305	0.8176
C13H3	0.0420	0.7225	0.7246

Table 10. Final atomic thermal parameters[1] for leptophos

Atom	β_{11}	β_{22}	β_{33}	β_{12}	β_{13}	β_{23}
Br	89(0)	200(1)	33(0)	-2(0)	13(0)	11(0)
Cl1	77(1)	216(3)	40(1)	-17(1)	-7(1)	7(1)
Cl2	75(1)	232(3)	43(1)	-20(1)	-2(1)	-16(1)
S	65(1)	250(3)	39(1)	25(1)	9(1)	-2(1)
P	57(1)	177(2)	29(0)	10(1)	4(0)	0(1)
O1	74(2)	185(6)	30(1)	18(3)	8(1)	10(2)
O2	74(3)	190(7)	49(2)	1(3)	-6(2)	-16(3)
C1	63(3)	156(9)	35(2)	14(4)	7(2)	4(3)
C2	54(3)	162(9)	39(2)	4(4)	7(2)	-8(3)
C3	70(3)	153(9)	38(2)	-3(4)	11(2)	1(3)
C4	68(3)	143(8)	33(2)	6(4)	12(2)	4(3)
C5	61(3)	137(8)	33(2)	9(4)	2(2)	3(3)
C6	57(3)	172(9)	37(2)	11(4)	5(2)	10(3)
C7	65(3)	172(9)	32(2)	-6(4)	8(2)	-1(3)
C8	84(4)	205(10)	32(2)	12(5)	6(2)	0(3)
C9	118(5)	223(12)	33(2)	3(6)	7(3)	3(4)
C10	129(5)	207(11)	39(2)	-26(6)	26(3)	-13(4)
C11	90(4)	211(11)	56(3)	-6(5)	30(3)	-15(5)
C12	74(4)	226(11)	45(2)	12(5)	12(2)	-2(4)
C13	108(5)	203(12)	61(3)	-4(6)	0(3)	-13(5)

[1]The hydrogen atoms were included with fixed isotropic thermal parameters $B_H = 4.5$.

Table 11. Bond distances (Å) in leptophos

P-S	1.911 (2)
P-O1	1.615 (3)
P-O2	1.579 (3)
O2-C13	1.420 (6)
P-C7	1.780 (4)
C7-C8	1.403 (6)
C8-C9	1.369 (7)
C9-C10	1.352 (8)
C10-C11	1.374 (8)
C11-C12	1.388 (7)
C12-C7	1.393 (7)
O1-C1	1.394 (5)
C1-C2	1.389 (6)
C2-C3	1.382 (6)
C3-C4	1.379 (6)
C4-C5	1.403 (6)
C5-C6	1.388 (6)
C6-C1	1.373 (6)
Cl1-C5	1.716 (4)
Cl2-C2	1.727 (4)
Br-C4	1.878 (4)

Table 12. Interatomic angles (°) in leptophos

S-P-O2	114.6(1)	P-O1-C1	121.0(3)
S-P-O1	116.9(1)	O1-C1-C2	119.7(4)
S-P-C7	116.8(1)	C1-C2-C3	120.1(4)
O1-P-O2	100.2(2)	C2-C3-C4	120.2(4)
O1-P-C7	99.8(2)	C3-C4-C5	119.8(4)
O2-P-C7	106.2(2)	C4-C5-C6	119.5(4)
P-O2-C13	123.0(3)	C5-C6-C1	120.3(4)
P-C7-C8	120.1(3)	C6-C1-C2	120.1(4)
C7-C8-C9	119.9(5)	C1-C2-C12	121.0(4)
C8-C9-C10	121.4(5)	C3-C2-C12	118.9(3)
C9-C10-C11	119.9(5)	C3-C4-Br	118.8(3)
C10-C11-C12	120.6(5)	C5-C4-Br	121.4(3)
C11-C12-C7	119.5(5)	C4-C5-Cl1	121.0(3)
C12-C7-C8	118.6(5)	C6-C5-Cl1	119.5(3)
C12-C7-P	121.1(4)		

Table 13. Least-squares planes[1] and deviations for leptophos

Atom	Distance from plane (Å)
Plane (I) defined by C1-C6, Br, Cl1, Cl2 and O1: (-0.51291)X + (0.85365)Y + (0.09051)Z = 2.76890	
Br	0.0001
Cl1	0.0355
Cl2	0.0247
O1	0.0242
C1	-0.0360
C2	-0.0089
C3	0.0037
C4	-0.0140
C5	-0.0064
C6	-0.0228
Plane (II) defined by C7-C12: (0.53995)X + (0.83200)Y + (0.12739)Z = 2.66205	
C1	-0.004
C8	0.006
C9	0.002
C10	-0.012
C11	0.014
C12	-0.005

[1]The planes are defined by $aX + bY + cZ - d = 0$, where X, Y and Z are coordinates along the Cartesian a, b and c axes.

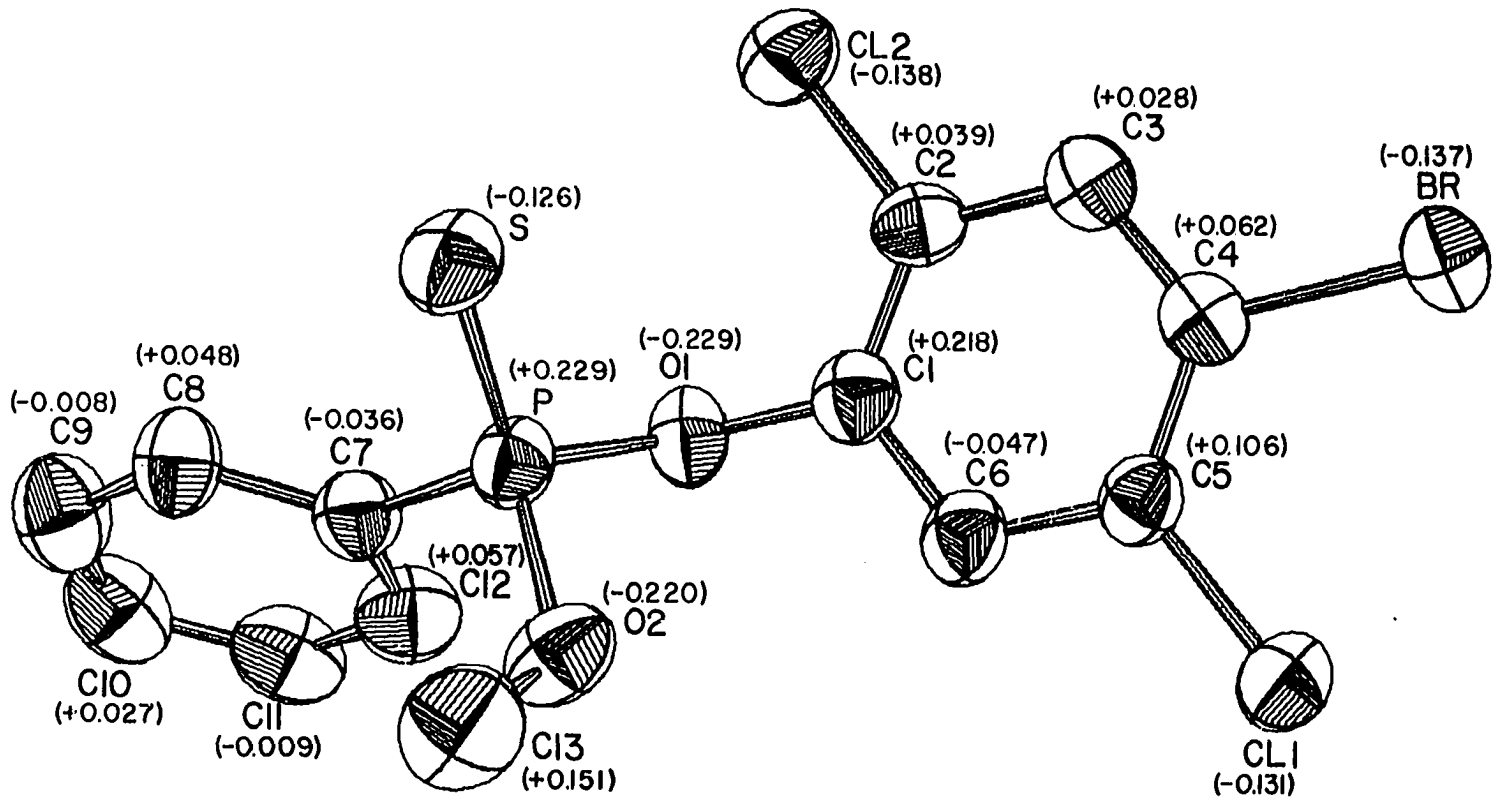

Figure 4. View of leptophos with partial charge densities obtained from CNDO/2 molecular orbital calculations. The thermal ellipsoids are drawn at the 50% probability level.

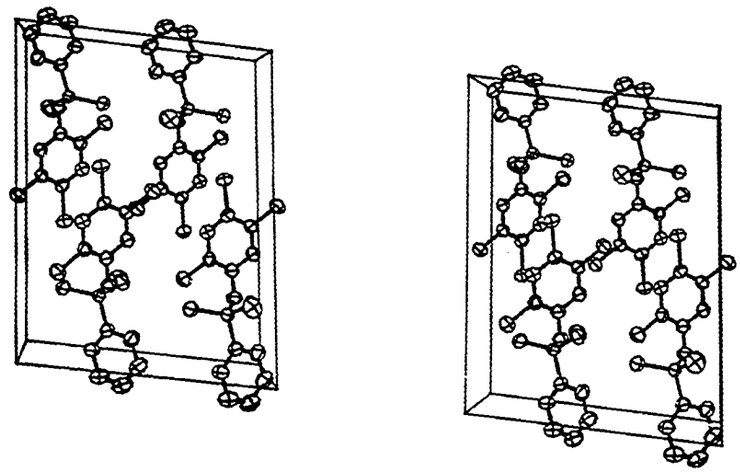

Figure 5. Unit cell stereograph of leptophos.

around the phosphorus are all less than tetrahedral. The P-O1 bond is 0.036 Å longer than the P-O2 bond while O1-C1 is 0.026 Å shorter than O2-C13. This would be consistent with a model in which the p_z orbital on O1 interacts with the aromatic ring system, thus strengthening the O1-C1 bond and weakening the O1-P bond. The P-O1, P-O2 and P=S bonds are all longer than the corresponding bonds in other phenoxy OP's. This is apparently a result of replacing an oxygen with a phenyl group on the phosphorus and the effect is similar to that found in the pyridoxy OP IPAT where an oxygen was replaced by nitrogen. Thus there are two factors in this molecule which contribute to a weakened P-O1 bond and this should be an important factor in enhancing the phosphorylating ability of insecticides.[32]

The position and orientation of the phosphate group are apparently determined primarily by intramolecular interactions. The phosphorus and Cl1 atoms lie on opposite sides of a plane perpendicular to the phenoxy ring and containing the O1-C1 bond. The C6-C1-O1-P torsion angle of 84.8° is representative of those found in other phenoxy OP's while the corresponding angle in the pyridoxy OP's is only 10°-30°, showing the steric effect of the hydrogen on C6. The S-Cl2 distance of 3.69 Å is only 0.04 Å greater than the sum of their van der Waals radii. The O2-H distance of 2.75 Å is only 0.15 Å greater than the sum of their van der Waals radii

and the P-O2...H and C13-O2...H angles of 98.0° and 129.3° indicate a nonbonding lobe on O2 directed toward the hydrogen, assuming sp^3 hybridization. Thus a weak electrostatic interaction may exist between the oxygen and hydrogen. These interactions would tend to restrict rotation about the P-O1 and C1-O1 bonds making the solid state configuration a likely in vivo model. In this configuration the P=S bond lies at an angle of 41.2° to the normal of the plane of the phenoxy group in close agreement with the range of 20°-40° usually observed in OP's. As in ronnel and bromophos this bond is slanted toward the Cl2 side of the phenoxy group.

In considering autotoxicosis through inhibition of AChE by organophosphorus insecticides, it is useful to recall that the nitrogen to carbonyl-carbon distance in acetylcholine is estimated at 4.7 Å when the molecule is in a proper configuration to react with bovine erythrocyte AChE.[17] The distance between anionic and esteratic sites of fly head AChE, however, may be as much as 1 Å longer than in the mammalian enzyme.[18] O'Brien[19] has reported a range of 4.5-5.9 Å for the insect AChE. A comparison of some intramolecular distances with these values should give some insight into the toxicity/activity of any insecticide. In addition to appropriate site separations, the two atoms involved must both have a net $\delta(+)$ charge to be in agreement with the AChE model of Krupka.[16]

CNDO/2 molecular orbital calculations[15] were carried out to compute approximate values for the charge density distribution in leptophos; the results are shown in Figure 4. Examination of this figure shows that some possible positive sites that could be involved in enzyme binding are located at C3, C4 and C5; H1, attached to C3 but not shown in the figure, is another possible site with a charge of +0.045e. The respective distances from the phosphorus are 4.76, 5.22, 4.66 and 5.47 Å. The P-C4 and P-C1 distances are too long for interaction with mammalian AChE but fall well within the range of acceptable distances for insect AChE. P-C3 and P-C5 distances, on the other hand, are acceptable to both insect and mammalian AChE. The charge on C3 is rather low to be very effective in binding to the enzyme but there is a possibility that the C3 and H1 atoms together form a region of $\delta(+)$ charge which provides a range of possible reactive sites.

THE CRYSTAL AND MOLECULAR STRUCTURE OF (-)-α-PHENYLETHYLAMMONIUM (-)-O-METHYL PHENYLPHOSPHONOTHIOATE

Experimental

Crystal Data A needle-shaped crystal with approximate dimensions 0.7 x 0.12 x 0.16 mm was mounted on a glass fiber and subsequently attached to a standard goniometer head. From four preliminary ω-oscillation photographs taken at various χ and ϕ settings, 14 independent reflections were selected and their coordinates were input to an automatic indexing algorithm.[3]

The resulting reduced cell and reduced cell scalars indicated orthorhombic symmetry. This was confirmed when oscillation photographs taken about all three axes displayed mirror symmetry. Observed layer line spacings were within experimental error of those predicted for this cell. The least-squares refinement of the lattice constants[4] based on the precise ±2θ measurements of 11 strong independent reflections, using Mo K_α radiation, λ = 0.70954 Å, at 27°C, yielded a = 15.611(7), b = 16.787(9) and c = 6.136(1) Å.

Collection and Reduction of X-Ray Intensity Data Data were collected at room temperature on an automated four-circle diffractometer designed and built in this laboratory.[5] The diffractometer is interfaced to a PDP-15 mini-

computer in a time-sharing mode and is equipped with a scintillation counter. Graphite-monochromated Mo K_α radiation was used for data collection.

All data (6739 reflections) were collected within a 2θ sphere of 50° in the hkl, $\bar{h}k\bar{l}$, $\bar{h}\bar{k}l$ and $h\bar{k}\bar{l}$ octants using an ω-scan data collection technique.

As a general check on electronic and crystal stability, the intensities of three standard reflections were remeasured every 75 reflections. These standard reflections were not observed to vary throughout the entire data collection period.

The intensity data were corrected for Lorentz-polarization effects but no absorption correction was made; the transmission factor was 0.89±0.07 with $\mu = 3.00$ cm^{-1}. The estimated variance in each intensity was calculated by:

$$\sigma_I^2 = C_T + k_t C_B + (0.03C_T)^2 + (0.03C_B)^2$$

where C_B and C_T represent the background and total counts, respectively, k_t is a counting time factor, and 0.03 is an estimate of nonstatistical errors. The estimated deviations in the structure factors were calculated by the finite-difference method.[7] Equivalent data were averaged and 1561 reflections with $F_o > 3.0\sigma(F)$ were retained for structural refinement.

Solution and Refinement

The observed extinction conditions h00: h=2n+1, 0k0: k=2n+1, and 00l: l=2n+1 uniquely determined the space group to be $P_{2_1}2_12_1$. The phosphorus and sulfur positions were determined by conventional Patterson techniques and the remaining nonhydrogen atoms were located by successive structure factor[43] and electron-density map[9] calculations. These atomic positions were subsequently refined by a block-diagonal least-squares procedure[43] minimizing the function $\Sigma\omega(|F_o| - |F_c|)^2$ where $\omega = 1/\sigma_F^2$. This refinement yielded a conventional residual index of $R = \Sigma||F_o| - |F_c||/\Sigma|F_o| = 0.088$. At this stage all 20 nonhydrogen atoms had been refined using anisotropic thermal parameters. The scattering factors used were those of Hanson *et al.*,[10] modified for the real and imaginary parts of anomalous dispersion.[11] The scattering factor for hydrogen was that of Stewart *et al.*[12]

Positions for the aromatic hydrogen atoms were calculated using a bond distance of 0.95 Å from the respective carbon atoms. Approximate positions for the methyl and amino hydrogens were obtained from an electron-density difference map and were refined by least-squares methods to be 1.0 Å from the respective carbon or nitrogen atoms with tetrahedral geometry. After a final cycle of full-matrix refinement, without varying the hydrogen parameters, the conventional residual index converged to R = 0.069. Low intensity

reflections caused a sharp increase in R at high angles and refinement using only the 1207 reflections with $2\theta \leq 45^{\circ}$ converged to R = 0.057.

The final positional and thermal parameters are listed in Tables 14 and 15, respectively. Standard deviations were calculated from the inverse matrix of the final least-squares cycle. Bond distances and angles[13] are listed in Tables 16 and 17, respectively.

Description and Discussion

A computer drawing of one molecule of the salt in the correct absolute configuration is shown in Figure 6, and a stereographic view of the contents of one unit cell is shown in Figure 7. As expected, both phenyl groups are strikingly planar (cf. Table 18).

In the phenylphosphonothioate ion the P=S bond lies nearly in the plane of the phenyl ring with a C6-C1-P-S torsional angle of only 2.9°. In the phenylethylammonium ion the C8-H bond lies nearly in the plane of the phenyl ring with a C15-C10-C8-H torsional angle of 10.3°. The two ions are held together primarily by weak electrostatic forces between hydrogen and oxygen or sulfur. The methyl and amino groups on the phenylethylammonium ion are both oriented with hydrogens pointed directly toward oxygen atoms on the other ion and the O-H(N) and O-H(C) distances of 2.12 and 2.56 Å,

Table 14. Final atomic positional parameters

Atom	x	y	z
S	0.3070(1)	0.1627(1)	0.4805(3)
P	0.37405(9)	0.12901(9)	0.2302(3)
O1	0.3577(3)	0.0458(2)	0.1554(9)
O2	0.3561(3)	0.1813(3)	0.0183(7)
N	0.1675(3)	0.1052(3)	0.243(1)
C1	0.4865(4)	0.1466(3)	0.276(1)
C2	0.5446(4)	0.1265(4)	0.112(1)
C3	0.6311(4)	0.1433(4)	0.135(2)
C4	0.6601(4)	0.1796(4)	0.318(2)
C5	0.6042(4)	0.1992(4)	0.485(2)
C6	0.5171(4)	0.1831(4)	0.463(1)
C7	0.3634(5)	0.2657(4)	0.027(2)
C8	0.1140(4)	0.0896(3)	0.212(1)
C9	0.1361(4)	0.1265(5)	0.993(1)
C10	0.0206(3)	0.0701(3)	0.236(1)
C11	0.9757(4)	0.0306(4)	0.075(1)
C12	0.8895(4)	0.0149(4)	0.102(2)
C13	0.8475(4)	0.0391(4)	0.283(2)
C14	0.8899(5)	0.0788(5)	0.442(1)
C15	0.9775(5)	0.0943(4)	0.424(1)
C2H	0.5238	0.1009	0.9838
C3H	0.6703	0.1296	0.0234
C4H	0.7200	0.1907	0.3329
C5H	0.6252	0.2243	0.6112
C6H	0.4780	0.1968	0.5744
C11H	0.0055	0.0138	0.9463
C12H	0.8593	0.9874	0.9929
C13H	0.7882	0.0283	0.2999
C14H	0.8608	0.0958	0.5681
C15H	0.0083	0.1217	0.5345
C7H1	0.3159	0.2874	0.1214
C7H2	0.4196	0.2805	0.0919
C7H3	0.3580	0.2881	0.8778
C9H1	0.1046	0.1780	0.9755
C9H2	0.1995	0.1373	0.9871
C9H3	0.1202	0.0893	0.8733
NH1	0.2264	0.0283	0.2285
NH2	0.1571	0.9938	0.3833
NH3	0.1523	0.9771	0.1349
C8H	0.1323	0.1315	0.3415

Table 15. Final atomic thermal parameters[1]

Atom	β_{11}	β_{22}	β_{33}	β_{12}	β_{13}	β_{23}
S	48(1)	68(1)	312(6)	-5(1)	19(2)	-30(2)
P	34(1)	31(1)	276(5)	-5(1)	-4(2)	-2(2)
O1	50(2)	40(2)	519(21)	-12(2)	-4(6)	-43(5)
O2	54(2)	67(2)	265(14)	-15(2)	-30(5)	34(5)
N	33(2)	36(2)	411(21)	-4(2)	3(6)	2(6)
C1	38(3)	27(2)	308(21)	-1(2)	-7(7)	5(6)
C2	41(3)	44(3)	370(24)	-2(2)	9(8)	0(8)
C3	42(3)	52(3)	581(34)	-2(3)	30(10)	-2(10)
C4	40(3)	37(3)	686(41)	-6(2)	-16(11)	10(10)
C5	50(4)	39(3)	514(31)	-1(2)	-68(11)	-22(9)
C6	43(3)	36(2)	385(26)	5(2)	-19(8)	-17(7)
C7	79(4)	46(3)	604(36)	-3(3)	-42(13)	79(10)
C8	36(3)	30(2)	346(23)	-2(2)	-28(7)	7(7)
C9	52(3)	63(4)	471(30)	-12(3)	-25(10)	71(10)
C10	38(3)	26(2)	299(21)	5(2)	-13(7)	6(6)
C11	42(3)	39(3)	375(26)	1(2)	-15(7)	-37(7)
C12	39(3)	43(3)	570(36)	-1(3)	-36(10)	-40(90)
C13	38(3)	46(3)	639(41)	5(3)	-3(11)	35(11)
C14	64(4)	63(4)	456(31)	18(3)	52(11)	29(10)

[1]The hydrogen atoms were included with fixed isotropic thermal parameters $B_H = 4.0$.

Table 16. Bond distances (Å)

P-S	1.943 (2)
P-O1	1.492 (4)
P-O2	1.594 (5)
P-C1	1.801 (6)
O2-C7	1.422 (8)
C1-C2	1.393 (9)
C2-C3	1.387 (9)
C3-C4	1.35 (1)
C4-C5	1.39 (1)
C5-C6	1.393 (9)
C6-C1	1.39 (1)
C8-C9	1.52 (1)
C8-N	1.516 (7)
C8-C10	1.502 (8)
C10-C11	1.384 (9)
C11-C12	1.382 (9)
C12-C13	1.35 (1)
C13-C14	1.35 (1)
C14-C15	1.39 (1)
C15-C10	1.40 (1)

Table 17. Interatomic angles (°)

S-P-O1	115.1(2)	C4-C5-C6	119.7(7)
S-P-O2	112.9(2)	C5-C6-C1	120.2(7)
S-P-C1	110.8(3)	C9-C8-N	108.7(6)
O1-P-O2	103.6(3)	C9-C8-C10	113.3(6)
O1-P-C1	111.6(2)	N-C8-C10	110.1(4)
O2-P-C1	102.0(3)	C8-C10-C11	121.7(6)
P-O2-C7	120.3(5)	C8-C10-C20	119.0(6)
P-C1-C2	118.9(5)	C11-C10-C15	119.2(6)
P-C1-C6	122.5(5)	C10-C11-C12	119.8(7)
C2-C1-C6	118.5(5)	C11-C12-C13	121.0(7)
C1-C2-C3	120.9(7)	C12-C13-C14	120.1(7)
C2-C3-C4	120.0(7)	C13-C14-C15	121.0(8)
C3-C4-C5	120.7(6)	C14-C15-C10	118.9(7)

Table 18. Least-squares planes[1] and deviations

Atom	Distance from plane (Å)
Plane (I) defined by C1-C6: (-0.14226)X + (0.89548)Y + (-0.42175)Z = 0.40542	
C1	0.004
C2	-0.004
C3	-0.002
C4	0.007
C5	-0.006
C6	0.001
Plane (II) defined by C10-C15: (0.21465)X + (-0.87149)Y + (0.44092)Z = 5.73870	
C10	0.0004
C11	-0.008
C12	0.007
C13	0.002
C14	-0.010
C15	0.008

[1]The planes are defined by aX + bY + cZ - d = 0, where X, Y and Z are coordinates along the Cartesian a, b and c axes.

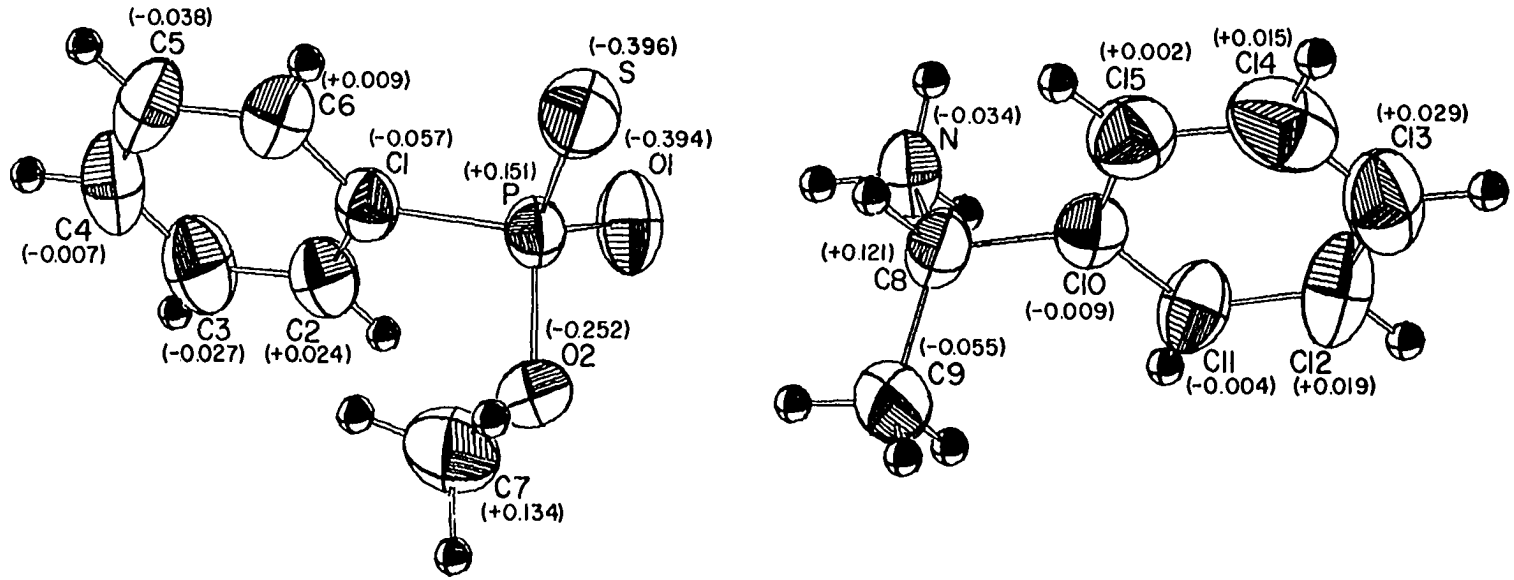

Figure 6. View of $PSO_2NC_{15}H_{20}$ with partial charge densities obtained from CNDO/2 molecular orbital calculations. The thermal ellipsoids are drawn at the 50% probability level.

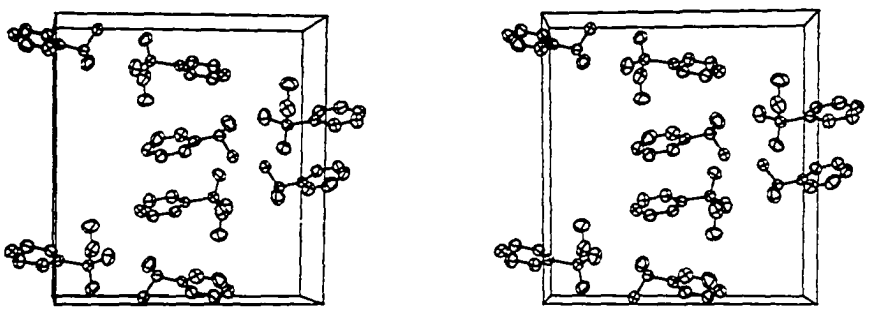

Figure 7. Unit cell stereograph of $PSO_2NC_{15}H_{20}$

respectively, are indicative of weak hydrogen bonds, particularly those involving nitrogen. The two phenyl rings are thus held in nearly coplanar positions, the dihedral angle between the two planes being 4.5°.

A comparison of bond distances and angles around the phosphorus atom with corresponding parameters in other organophosphorus molecules yields some interesting results. Since O1 is not bonded to an aromatic ring, it would be expected to show a much stronger bond to the phosphorus, and indeed a bond length of 1.492 Å is found compared to 1.615 Å in leptophos, 1.607 Å in bromophos[22] and 1.592 Å in ronnel.[21] The other three bond lengths involving phosphorus are correspondingly larger than in leptophos: 1.943(2) vs. 1.911(2) Å for P=S, 1.594(5) vs. 1.579(3) Å for P-O2, and 1.801(6) vs. 1.780(4) Å for P-C1. Direct comparisons of these distances cannot be made for the other molecules because of the substitution of the phenyl ring with oxygen or nitrogen, but it should be noted that 1.923 Å for IPAT is the longest P=S bond and 1.579 Å for leptophos is the longest P-O2 bond observed in the series of OP's studied in this laboratory.

The angles around the phosphorus range from 102.0° to 115.1° making the distortion from tetrahedral geometry smaller than in leptophos (99.8° to 116.9°). All angles of the type S=P-X (X = O or C) are smaller than in leptophos but still larger than the tetrahedral angle. The greatest change

in angle involves O1-P-C1 which is 11.8° larger in the salt than in leptophos. In general the changes in bond angles appear to be primarily due to changes in the P=S and P-O1 distances, i.e., as the sulfur gets closer to the phosphorus the remaining three atoms on the phosphorus are displaced causing increased P=S-X angles.

THE CRYSTAL AND MOLECULAR STRUCTURES OF CALCIUM FORMATE

Introduction

The first x-ray analyses of calcium formate were those of Nitta[44] who determined that the C-O distances are equal (ca. 1.25 Å) and that the O-C-O angle is 124° in the formate ion. Schutte and Buijs[45] discovered that a second phase of calcium formate crystallizes when a water-miscible organic solvent is added to an aqueous solution of $Ca(HCOO)_2$ and called this phase β-$Ca(HCOO)_2$ to distinguish it from α-$Ca(HCOO)_2$ which crystallizes from aqueous solution. They also reported that the β phase had been obtained along with the α form by rapid crystallization from aqueous solution at 90°C and that it was unstable in contact with the atmosphere. Their studies of the infrared spectra of both forms revealed that the α form has two unique formate ions indicated by a doubling of all the bands. The β form, on the other hand, contains only one unique formate ion giving rise to a single set of bands in the infrared spectrum. Donaldson, Knifton, and Ross[46] also studied the infrared spectrum of α-$Ca(HCOO)_2$ and concluded that the Ca-O bonds are ionic. Comel and Mentzen[47] studied phase transitions via differential thermal analysis and concluded that the α form is thermodynamically more stable than the β form at room temperature.

Recently, Vaughan[48] has been developing a solid state nuclear magnetic resonance technique for determining atomic positions in crystalline structures, and selected calcium formate as a standard crystal to test his methods. However, when attempting to interpret the results of his experiments the hydrogen atom appeared to be oscillating between two widely separated positions in the plane of the formate ion. Since precise structural data were not available at that time we decided to investigate the behavior of the hydrogen atom via diffraction techniques. Our original plan was to obtain precise nonhydrogen parameters by x-ray methods and to follow this by a determination of the hydrogen position with neutron diffraction data.

The calcium formate structure was also used as a test case for a new data collection algorithm designed to improve the accuracy of low intensity reflections. The estimated variance in the intensity of a reflection is given by

$$\sigma_I^2 = C_T + k_t C_B + (0.03C_T)^2 + (0.03C_B)^2 \qquad (1)$$

where C_T and C_B are the total and background counts and k_t is a counting time factor. From this equation it can be seen that the relative error in a measurement increases as the number of counts decreases. It follows that the accuracy of an intensity measurement can be improved by increasing the number of counts. For very intense reflections, however, such an increase is not necessary and may even be detrimental

if it causes the counting buffer to overflow. Therefore, a multiple scan technique was developed in which the computer compares the total counts for a reflection to some minimum value. If the count is below this minimum the scan is repeated and the new count added to the previous total until the preset minimum count is reached. In order to avoid the computer spending too much time on very low intensity or extinct reflections no scan is repeated more than ten times. The intensity of the peak is then the average value for all the scans and the variance is given by

$$\sigma_I^2 = C_T + \left(\frac{n_s}{n_c k_t} C_B\right) + \left(\frac{0.03}{n_c} C_T\right)^2 + \left(\frac{0.03 n_c k_t C_B}{n_s}\right)^2 \qquad (2)$$

where n_s = number of steps

n_c = number of scans

and k_t = counting time factor.

Calcium formate was prepared by neutralizing a solution of formic acid with calcium hydroxide. The α form was obtained by crystallization at room temperature and the β form by recrystallization from aqueous solution at 90°C. Two sets of data were collected for the α form; one by standard techniques and one by the multiple scan technique.

α-Calcium Formate

A spherical crystal approximately 0.4 mm in diameter was selected and mounted on the end of a glass fiber with Duco cement and subsequently attached to a standard goniometer head. From four preliminary ω-oscillation photographs taken at various χ and ϕ settings, 12 independent reflections were selected and their coordinates were input to an automatic indexing algorithm.[3]

The resulting reduced cell and reduced cell scalars indicated orthorhombic symmetry. This was confirmed by axial oscillation photographs which revealed mirror symmetry for all three axes. Observed layer line spacings were within experimental error of those predicted for this cell. The lattice constants for this cell, using Mo K_α radiation, λ = 0.70954 Å, at 27°C, are $\underline{a}$ = 10.168, $\underline{b}$ = 13.407 and $\underline{c}$ = 6.278 Å, with Z = 8.

Data were collected at room temperature on an automated four-circle diffractometer designed and built in this laboratory.[5] The diffractometer is interfaced to a PDP-15 minicomputer in a time-sharing mode and is equipped with a scintillation counter. Graphite-monochromated Mo K_α radiation was used for data collection.

All data (4345 reflections) within a 2θ sphere of 55° were measured in the hkl, $hk\bar{l}$, $h\bar{k}l$ and $h\bar{k}\bar{l}$ octants using a standard ω-scan data collection technique.

As a general check on electronic and crystal stability, the intensities of three standard reflections were remeasured every 75 reflections. These standard reflections were not observed to vary throughout the entire data collection period. An examination of the data revealed systematic absences for 0kl: l≠2n, h0l: h≠2n and hk0: k≠2n, and the space group was determined to be P_{cab}.

The intensity data were corrected for Lorentz and polarization effects but no absorption correction was made; with $\mu = 10.87\ cm^{-7}$ the transmission factor was 0.65. The estimated variance in each intensity was calculated by Equation (1) and the estimated standard deviations in the structure factors were calculated by the finite-difference method.[7] Equivalent data were averaged and 936 reflections with $F_o > 3.0\sigma(F)$ were retained for structural refinement.

A second set of data was then collected on the same crystal using the multiple ω-scan technique. For this test the minimum intensity for a peak was set at 20000 and the counting time for each step was increased to 0.10 sec. from its usual value of 0.05 sec. All data (2206 reflections) were collected within a 2θ sphere of 55° in the hkl and hk$\bar{l}$ octants.

Six standard reflections were monitored to check crystal and electronic stability and once again no significant change was observed throughout the data collection period.

As before the intensity data were corrected for Lorentz and polarization effects but not for absorption. The estimated variance in each intensity was calculated by Equation (2) and the estimated standard deviations in the structure factors were calculated by the finite-difference method. Equivalent data were averaged and 943 reflections with $F_o > 3.0\sigma(F)$ were retained for structural refinement.

All nine nonhydrogen atoms were located by MULTAN[29] using the second set of data. These positions were subsequently refined by a full-matrix least-squares procedure[8] minimizing the function $\Sigma\omega(|F_o| - |F_c|)^2$ where $\omega = 1/\sigma_F^2$. This refinement yielded a conventional residual index of $R = \Sigma||F_o| - |F_c||/\Sigma|F_o| = 0.071$ and 0.065 for the first and second data sets, respectively, and a weighted residual of $\omega R = \Sigma\omega||F_o| - |F_c||/\Sigma\omega|F_o| = 0.087$ and 0.079, respectively. Thus the multiple scan data did appear to be better than the standard data and was used for the final stages of refinement. The scattering factors used were those of Hanson et al.,[10] modified for the real and imaginary parts of anomalous dispersion.[11] The scattering factor for hydrogen was that of Stewart et al.[12]

The positions of the hydrogen atoms were determined by examination of an electron-density difference map. The positions and isotropic temperature factors of the hydrogen atoms were allowed to refine and the R factor converged to 0.060.

At this point a small secondary extinction effect was noted and a correction was applied on the basis of equations derived by Darwin.[49] The observed and calculated intensities are related by the expression

$$I_o = I_c \exp(-2gI_c) \tag{3}$$

where g is a secondary extinction coefficient. Rewriting Equation (3) and expanding the exponential as a series to first order in I_c results in

$$I_c/I_o = 1 + 2gI_c \tag{4}$$

Using the five largest reflections and solving Equation (4) for g yielded an average value of 1.13×10^{-5}. This was then used to modify the observed structure factors according to the equation

$$|F_c| = |F_o|(1 + gI_c). \tag{5}$$

After two more cycles of refinement the R factor converged to 0.049 and $\omega R = 0.056$.

The final positional and thermal parameters are listed in Table 19. Standard deviations were calculated from the inverse matrix of the final least-squares cycle. Bond lengths and angles for the formate ions are listed in Table 20 and selected angles around the Ca^{++} ion are listed in Table 21.

Table 19. Final atomic positional[1] and thermal[2] parameters for α-$Ca(HCOO)_2$

Atom	x	y	z	β_{11}	β_{22}	β_{33}	β_{12}	β_{13}	β_{23}
Ca	0.13428(3)[3]	0.89251(2)	0.97221(5)	40(1)	26(1)	116(2)	0(1)	-2(1)	-4(1)
O1	0.2992(1)	-0.01484(8)	0.1327(2)	73(1)	45(1)	186(3)	-18(1)	-26(1)	1(1)
O2	0.4638(1)	0.04722(8)	0.3100(2)	70(1)	41(1)	178(3)	-14(1)	-31(2)	1(1)
O3	0.0235(1)	0.2016(1)	0.2120(2)	65(1)	45(1)	165(3)	-17(1)	0(1)	-5(1)
O4	0.2000(1)	0.29850(8)	0.2148(2)	58(1)	34(1)	151(3)	-9(1)	2(1)	-9(1)
C1	0.3870(2)	0.0488(1)	0.1565(3)	65(1)	32(1)	140(4)	-6(1)	-12(2)	9(1)
C2	0.1257(1)	0.2343(1)	0.1334(3)	56(2)	33(1)	129(4)	-6(7)	3(1)	-7(1)
H1	0.159(2)	0.205(2)	0.002(4)	138(43)					
H2	0.404(2)	0.108(2)	0.054(5)	157(53)					

[1]The positional parameters for all atoms are represented in fractional unit cell coordinates.

[2]The β_{ij} are defined by: $T = \exp[-(h^2\beta_{11} + k^2\beta_{22} + l^2\beta_{33} + 2hk\beta_{12} + 2hl\beta_{13} + 2kl\beta_{23})]$. If only the β_{11} column is listed this corresponds to an isotropic temperature factor. Nonhydrogen thermal parameters are ($\times 10^4$), hydrogen thermal parameters are ($\times 10^2$).

[3]In this and succeeding tables, estimated standard deviations are given in parentheses for the least significant figures.

Table 20. Bond distances (Å) and angles (°) in the formate ions

C1-O1	1.245(2)	C2-O3	1.231(2)
C1-O2	1.240(2)	C2-O4	1.254(2)
C1-H2	1.03(5)	C2-H1	0.98(5)
O1-C1-O2	122.2(2)	O3-C2-O4	126.2(2)
H2-C1-O1	124.7(9)	H1-C2-O3	119.2(9)
H1-C1-O2	113.0(9)	H1-C2-O4	114.4(9)

Table 21. Selected angles (°) around the Ca^{++} ion[1]

O1-Ca-O2	89.20(5)	O3-Ca-O4	88.11(5)
O1-Ca-O4	95.53(5)	O3-Ca-O1'	91.79(4)
O1-Ca-O4'	74.16(4)	O3-Ca-O2'	88.44(5)
O1-Ca-O1'	84.89(4)	O3-Ca-O3'	70.04(4)
O1-Ca-O2'	91.21(5)	O4-Ca-O3'	71.21(4)
O2-Ca-O3	87.53(4)	O4-Ca-O4'	84.87(4)
O2-Ca-O3'	96.95(4)	O4-Ca-O2'	70.10(4)
O2-Ca-O4'	86.01(4)	O1'-Ca-O2'	50.76(4)
O2-Ca-O1'	70.30(4)	O3'-Ca-O4'	40.01(3)
C2-Ca-O1	92.16(4)	C1-Ca-O1	87.95(4)
C2-Ca-O2	92.78(4)	C1-Ca-O2	95.60(4)
C2-Ca-O3	90.34(4)	C1-Ca-O3	90.03(4)
C2-Ca-O4	76.25(4)	C1-Ca-O4	95.38(4)

[1]C1, O1' and O2' and C2, O3' and O4' are the axial ions.

Table 22. Least-squares planes[1] and deviations for α-$Ca(HCOO)_2$

Atom	Distance from plane (Å)
Plane (I) defined by O1, O2, C1 and H1: (0.63259)X + (0.56863)Y + (0.52581)Z = 10.9	
O1	0.0003
O2	0.0002
C1	-0.0009
H1	0.0003
Plane (II) defined by O3, O4, C2 and H1: (-0.50333)X + (0.70273)Y + (0.50281)Z = 10.6	
O3	-0.0080
O4	-0.0076
C2	0.0247
H1	-0.0090

[1]The planes are defined by $aX + bY + cZ - d = 0$, where X, Y and Z are coordinates along the Cartesian a, b and c axes.

Figure 8. The coordination sphere around the Ca^{++} ion in α-$Ca(HCOO)_2$ showing 50% probability ellipsoids.

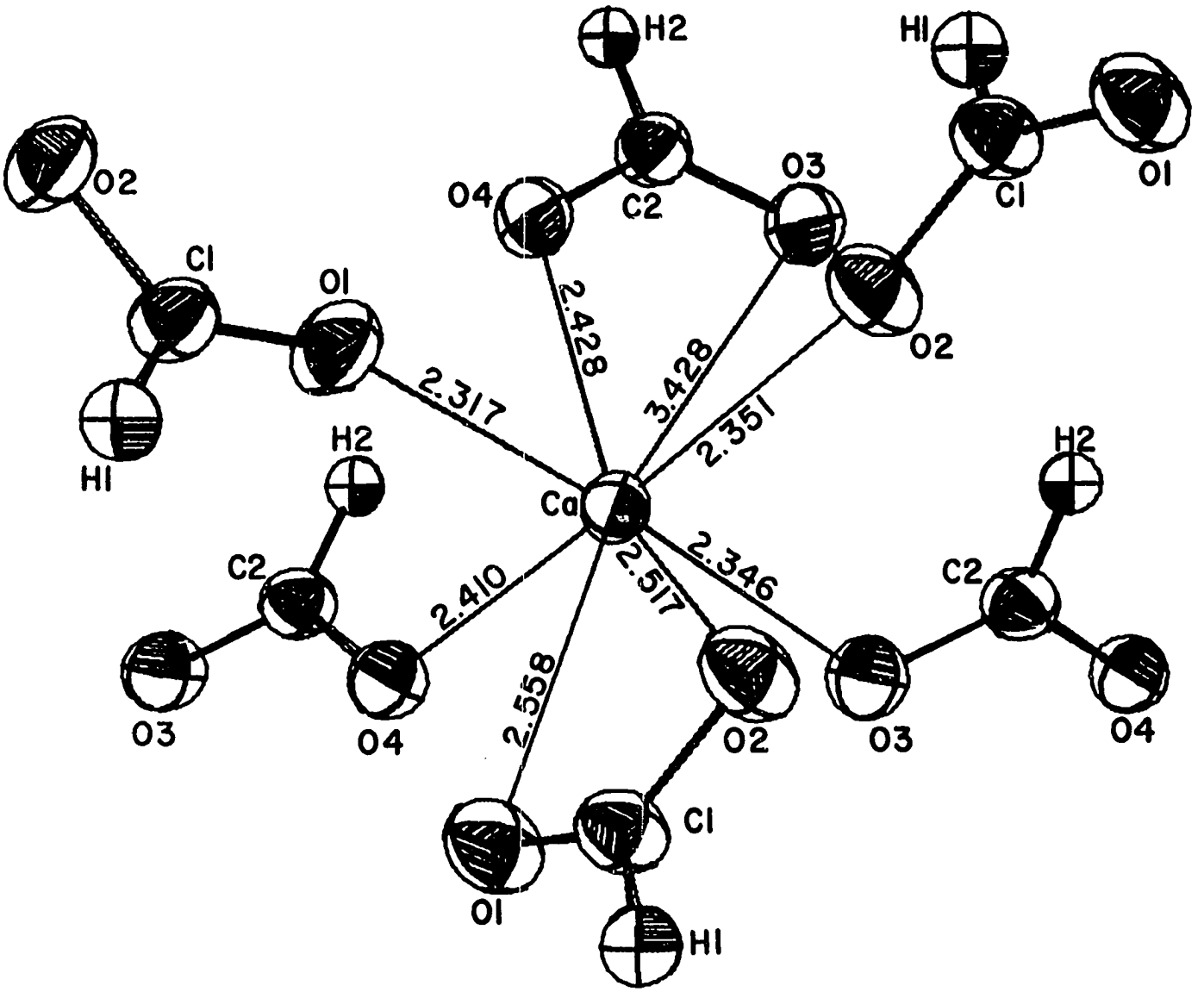
H2
H1
O2
O4
C2
O3
Cl
O1
Cl
O1
2.428
3.428
2.317
2.351
O2
H1
H2
Ca
H2
C2
2.410
2.517
2.346
C2
2.558
O3
O4
O2
O3
O4
Cl
O1
H1

β-Calcium Formate

An octahedral crystal 0.4 mm on a side was selected and mounted on the end of a glass fiber with Duco cement and subsequently attached to a standard goniometer head. From four preliminary ω-oscillation photographs taken at various χ and ϕ settings, 10 independent reflections were selected and their coordinates were input to an automatic indexing algorithm.[3]

The resulting reduced cell and reduced cell scalars indicated tetragonal symmetry. This was confirmed by axial oscillation photographs which revealed mirror symmetry for all three axes. Observed layer line spacings were within experimental error of those predicted for this cell. The lattice constants obtained from the precise ±2θ measurements of 12 strong independent reflections, using Mo K_α radiation, λ = 0.70954 Å, at 27°C, are $\underline{a}$ = 6.765(2) and $\underline{c}$ = 9.456(3) Å, with Z = 4.

Data were collected at room temperature on an automated four-circle diffractometer designed and built in this laboratory.[5] Graphite-monochromated Mo K_α radiation was used for data collection.

All data (1150 reflections) within a 2θ sphere of 55° were measured in the hkl and hk$\bar{l}$ octants using a standard ω-scan technique. However, the data were collected with the b axis unique and upon completion of data collection the

indices were transformed to

$$\begin{pmatrix} h' \\ k' \\ l' \end{pmatrix} = \begin{pmatrix} -1 & 0 & 0 \\ 0 & 0 & 1 \\ 0 & 1 & 0 \end{pmatrix} \begin{pmatrix} h \\ k \\ l \end{pmatrix} .$$

As a general check on electronic and crystal stability, the intensities of three standard reflections were remeasured every 75 reflections. These standard reflections were not observed to vary throughout the entire data collection period.

The intensity data were corrected for Lorentz and polarization effects. Since $\mu = 10.87$ cm^{-1} no absorptions corrections were made; minimum and maximum transmission factors were 0.63±0.07. The estimated variance in each intensity was calculated by Equation (1). The estimated standard deviations in the structure factors were calculated by the finite-difference method.[7] Equivalent data were averaged and 565 reflections with $F_o > 3.0\sigma(F)$ were retained for structural refinement.

A statistical test of the data[6] indicated an acentric space group and the observed extinction conditions, 001: $l \neq 4n$ and h00: $h \neq 2n$, indicated the space group $P_{4_1 2_1 2}$.

The calcium position was determined by analysis of a sharpened three-dimensional Patterson function and the other nonhydrogen positions were located on successive electron-density maps. The position of the hydrogen atom was obtained

from a difference electron-density map. These positions were subsequently refined by a full-matrix least-squares procedure[8] minimizing the function $\Sigma\omega(|F_o| - |F_c|)^2$ where $\omega = 1/\sigma_F^2$. All nonhydrogen atoms were refined anisotropically and the hydrogen atom was refined isotropically to a conventional residual index of $R = \Sigma||F_o| - |F_c||/\Sigma|F_o| = 0.070$. A small secondary extinction effect was noted and the structure factors were modified according to Equation (5) using $g = 1.21 \times 10^{-5}$. After this correction the conventional residual index converged to R = 0.044. The scattering factors used were those of Hanson et al.,[10] modified for the real and imaginary parts of anomalous dispersion.[11] The hydrogen scattering factor was that of Stewart et al.[12]

The final positional and thermal parameters are listed in Table 23. Standard deviations were calculated from the inverse matrix of the final least-squares cycle. Bond lengths and angles for the formate ion are listed in Table 24 and selected angles around Ca^{++} are listed in Table 25.

Description and Discussion

The coordination spheres around the Ca^{++} ion are shown in Figures 8 and 9 for the α and β forms, respectively. The structure of α-$Ca(HCOO)_2$ by neutron diffraction analysis[50,51] was reported at the same time that this x-ray study was completed and the reported interatomic distances and angles are

Table 23. Final atomic positional[1] and thermal[2] parameters for β-$Ca(HCOO)_2$

Atom	x	y	z	β_{11}	β_{22}	β_{33}	β_{12}	β_{13}	β_{23}
Ca	0.2172(2)[3]	0.2172(2)	0.0(0)	95(1)	95(1)	89(1)	-1(1)	-11(1)	11(1)
O1	0.5651(3)	0.2233(3)	-0.0154(2)	126(4)	203(5)	96(2)	11(3)	-9(2)	-4(3)
O2	-0.1202(3)	0.2194(3)	0.0348(3)	104(4)	288(6)	187(3)	-15(3)	16(3)	11(4)
C	0.1963(4)	0.7060(3)	-0.0674(3)	185(6)	118(5)	77(2)	-22(4)	7(3)	-10(3)
H	0.104(4)	0.704(4)	-0.1603(3)	176(65)					

[1]The positional parameters for all atoms are represented in fractional unit cell coordinates.

[2]The β_{ij} are defined by: $T = \exp[-(h^2\beta_{11} + k^2\beta_{22} + l^2\beta_{33} + 2hk\beta_{12} + 2hl\beta_{13} + 2kl\beta_{23})]$. If only the β_{11} column is listed this corresponds to an isotropic temperature factor. Nonhydrogen thermal parameters are ($\times 10^4$), hydrogen thermal parameters are ($\times 10^2$).

[3]In this and succeeding tables, estimated standard deviations are given in parentheses for the least significant figures.

Table 24. Bond distances (Å) and angles (°) in the formate ion

C-O1	1.247(3)	O1-C-O2	123.9(3)
C-O2	1.225(3)	O1-C-H	125.9(1.4)
C-H	1.08(3)	O2-C-H	107.0(1.4)

Table 25. Selected angles (°) around the Ca^{++} ion[a]

$O1-Ca-O2^{1}$	90.11(5)	$O2-Ca-O1^{1}$	90.11(5)
$O1-Ca-O1^{1}$	88.21(9)	$O2-Ca-O1^{2}$	92.05(8)
$O1-Ca-O2^{3}$	64.38(7)	$O2-Ca-O2^{2}$	90.64(9)
$O1-Ca-O1^{2}$	84.29(8)	$O2-Ca-O1^{3}$	73.49(8)
$O1-Ca-O2^{2}$	84.52(6)	$O1^{1}-Ca-O1^{3}$	88.29(8)
$O2^{1}-Ca-O2$	91.9(1)	$O1^{1}-Ca-O2^{3}$	84.52(5)
$O2^{1}-Ca-O1^{3}$	92.05(8)	$O1^{1}-Ca-O2^{2}$	64.38(7)
$O2^{1}-Ca-O2^{3}$	90.64(9)	$O1^{2}-Ca-O2^{2}$	46.51(6)
$O2^{1}-Ca-O1^{2}$	73.49(8)	$O1^{3}-Ca-O2^{3}$	46.51(6)
C-Ca-O1	87.74(6)	$C^{1}-Ca-O1$	82.54(7)
$C-Ca-O2^{1}$	92.84(8)	$C^{1}-Ca-O2^{1}$	96.57(8)
C-Ca-O2	96.57(8)	$C^{1}-Ca-O2$	92.84(8)
$C-Ca-O1^{1}$	82.54(7)	$C^{1}-Ca-O1^{1}$	87.74(7)

[a]The oxygen atoms are related by the symmetry operations x,y,z; y,x,z; 0.5-y,0.5+x,0.25+z; and 0.5+x,0.5-y,-0.25-z. C, $O1^{3}$ and $O2^{3}$ and C^{1}, $O1^{2}$ and $O2^{2}$ are the axial formate ions.

Table 26. Least squares plane[1] of the formate ion in β-$Ca(HCOO)_2$

Atom	Distance from plane (Å)
Plane defined by O1, O2, C and H: (0.87344)X + (-0.09346)Y + (-0.47786)Z = 0.92512	
O1	0.0003
O2	0.0002
C1	-0.0009
H1	0.0003

[1]The plane is defined by aX + bY + cZ - d = 0, where X, Y and Z are coordinates along the Cartesian a, b and c axes.

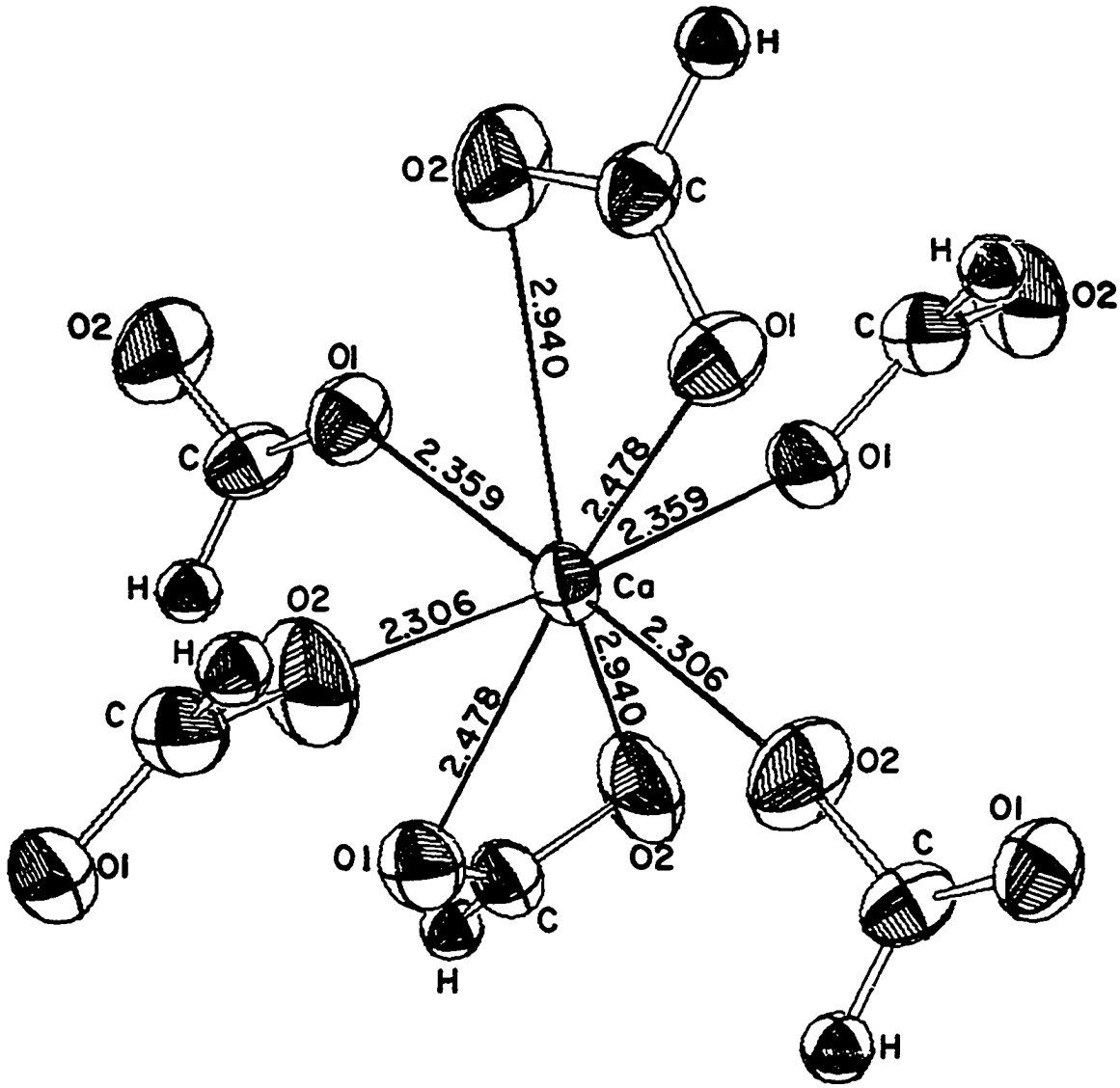

Figure 9. The coordination sphere around the Ca^{++} ion in β-calcium formate. The ellipsoids are at the 50% probability level.

in very close agreement with our results.

The geometry around the Ca^{++} ion in both forms may be described as distorted octahedral with oxygen atoms at the four equatorial positions and a formate ion coordinated in a bidentate fashion at each axial position. An examination of Tables 21 and 25 shows that all angles involving C1 and C2 with O1, O2, O3 and O4 in the α form and C and C' with O1, O2, O1' and O2' in the β form are in the range of 90°±7.5° with one exception (C2-Ca-O4 for α is 76.3°). The orientations of the formate ions are different in the two forms, however. If one considers the planes defined by the carbon and oxygens in each ion, then the two axial ions in the α form have a dihedral angle of 70° while the axial formate ions in the β form are perpendicular to each other.

The average C-O distance in each formate ion of the α form is 1.243 Å compared to 1.236 Å in the β form. In the infrared spectra[4,5] the symmetric C-O stretch mode produces two bands with an average frequency of 1357.5 cm^{-1} in the α form and a single band at 1359 cm^{-1} in the β form. These are very small differences but the shorter bond length and higher stretching frequency both indicate a slightly stronger C-O bond in the β form. At the same time the C-H stretching frequencies of both formate ions in the α form (2869 and 2890 cm^{-1}) are higher than the corresponding band in the β form (2857 cm^{-1}) and both C-H bond lengths in the α form (1.03 and

0.98 Å) are shorter than in the β form (1.08 Å). Hence as the C-O bonds get stronger, the C-H bonds get weaker in transforming from α to β.

A closer examination of the geometries of the formate ions also yields some interesting results. In the α form one formate ion has almost identical C-O bond lengths (1.245 and 1.240 Å) while in the other ion the C-O bonds differ by 0.017 Å. The first ion is strikingly planar (cf. Table 22), the greatest deviation from the plane being 0.0009 Å, while the second ion is slightly distorted, the deviations from the plane being 30 times greater than for the first ion but still on the order of experimental error. In the β form the C-O bond lengths differ by 0.022 Å and the deviations from the least squares plane (cf. Table 26) are three times larger than in the second ion of the α form. This deviation from planarity, along with the changes in bond lengths, suggests that the formate ion is under some strain in the β form.

The average Ca-O distance in the β form (2.521 Å) is also shorter than in the α form (2.544 Å). This is especially interesting in view of the fact that the total cell volume per formula unit for each form (107.0 $Å^3$ for α, 108.2 $Å^3$ for β) indicates a lower density for the β form. With the atoms lying closer together in spite of a greater available volume, the β form can be seen to have less efficient packing and a less stable configuration than the α form in agreement

with the DTA results of Comel and Mentzen.[47]

In conclusion the geometry around the Ca^{++} ions of both forms are quite similar. The crystal structures of calcium formate correlate completely with reported spectroscopic studies. The hydrogen shows no unexpected behavior within the crystal and indeed the parameters obtained were sufficiently informative that the neutron diffraction study was deemed unnecessary. Although the β form is less stable than the α form at room temperature, it is stable in contact with the atmosphere over the period of time (days) required for a single crystal diffraction study. The stability of the β form and the relative ease of producing it from aqueous solution contradicted the characteristics implied in the literature. In subsequent communications with Vaughan it was learned that his calcium formate was produced by both slow and rapid evaporation from aqueous solutions and hence was a mixture of both crystalline forms. Thus the anomalous results for the hydrogen positions were due to the different environments of hydrogen in the two forms.

LEAST-SQUARES REFINEMENT OF STRUCTURAL PARAMETERS

Introduction

A new program, called ALLS, has been written in FORTRAN to perform the least-squares refinement of crystal structure parameters based on single crystal x-ray diffraction data. A listing of the program and detailed instructions for its use are provided elsewhere.[43]

This program performs successive cycles of refinement using either the full-matrix or block-diagonal matrix of the normal equations. The parameters which may be refined include an overall scale factor, a secondary extinction coefficient, individual atom multipliers, atomic coordinates and isotropic or anisotropic temperature factors. The parameters to be varied are specified in the input and different parameters may be varied in each cycle. Structures of any symmetry can be accommodated by special subroutines. The observations may be weighted individually or the use of unit weights may be specified.

The program is an extension of the ORFLS program[8] in that it uses the same methods to handle symmetry, calculate derivatives, and invert the matrix. A major goal in the development of ALLS, however, was to improve the efficiency of structural refinement and to increase the generality of the program. Towards this goal several significant modifica-

tions were made. A major addition was the provision for either block-diagonal or full-matrix refinement. Block-diagonal refinement is considerably more efficient than full-matrix refinement if one can assume that the atom-atom interactions that it neglects are essentially insignificant. For this assumption to be valid some interaction between the scale factor and atomic temperature factors must be included, however, and some programs in the past have accomplished this by introducing an overall temperature factor and letting this interact with the scale factor. Even with such an inclusion, block-matrix approaches in the past have been hampered by overshifting, especially in the early stages of refinement, and damping factors have had to be applied to the calculated shifts. In order to circumvent this difficulty, a new block-diagonal approach has been devised which has been found to work quite well without using either the overall temperature factor or damping factors.

Two other options which may be used to decrease the number of computations required are reuse of the matrix and truncation of the data set. ALLS calculates the elements of the matrix in the first cycle of a job, but if the calculated shifts are less than ten times the estimated error for all the parameters and the full-matrix is being used, it does not recalculate them in following cycles. The user can override this option but our experience indicates that this is

generally not necessary.

Since the matrix elements are sums over all the reflections, the number of calculations can be further decreased by reducing the number of reflections used. In particular, in the early stages of refinement, relatively low resolution is usually required and hence the data set can be limited to the low angle reflections. As one seeks to improve the resolution in the structure, more data can be included by increasing the maximum value of $\sin\theta/\lambda$ to be allowed. All data at higher angles will be neglected in the refinement.

Other modifications to the program include the options to output either regular or sharpened coefficients for an electron-density map calculation, to refine a secondary extinction coefficient and to refine different parameters in succeeding cycles.

Mathematical Background

The Block-Diagonal Method The method of least-squares as applied in crystallography commonly minimizes the function:

$$D = \sum_r \omega_r (|F_{or}| - |sF_{cr}|)^2 \qquad (1)$$

where the sum is taken over all reflections,

$$|sF_{cr}| = (A_{cr}^2 + B_{cr}^2)^{1/2} \qquad (2)$$

where

$$A_{cr} = s\sum_i f_i a_i \cos 2\pi (hx_i + ky_i + lz_i) T_i \qquad (3)$$

and

$$B_{cr} = s\Sigma_i f_i a_i \sin 2\pi (hx_i + ky_i + lz_i) T_i \qquad (4)$$

and ω_r is the weight associated with each observation. For isotropic thermal motion

$$T_i = \exp(-B_i \sin^2\theta/\lambda^2) \qquad (5)$$

and for anisotropic thermal motion

$$T_i = \exp[-(h^2\beta_{11_i} + k^2\beta_{22_i} + l^2\beta_{33_i} + 2hk\beta_{12_i} + 2hl\beta_{13_i} + 2kl\beta_{23_i})] \qquad (6)$$

Minimization of Equation (1) is achieved by differentiating with respect to each parameter and equating to zero. This leads to n equations of the form

$$\Sigma_r \omega_r (|F_{or}| - |sF_{cr}|)\partial |sF_{cr}(p_1 \cdots p_n)|/\partial p_j = 0. \qquad (7)$$

Since $|sF_{cr}|$ is nonlinear in all parameters except s we will express it as a Taylor series and neglect second and higher powers, so that

$$|sF_{cr}(p_1 \cdots p_n)| = |sF_{cr}(a_1 \cdots a_n)| + \Sigma_i (\partial |sF_{cr}|/\partial p_i)\Delta p_i \qquad (8)$$

where $p_1 \cdots p_n$ may be any scale, positional or thermal parameters and

$$\Delta p_i = p_i - a_i.$$

Substitution of Equation (8) into Equation (7) and rearrangement of terms leads to

$$\Sigma\Sigma_{ir} \omega_r (\partial |sF_{cr}|/\partial p_j)(\partial |sF_{cr}|/\partial p_i)\Delta p_i = \Sigma_r \omega_r (\partial |sF_{cr}|/\partial p_j)\Delta F_r \qquad (9)$$

where $\Delta F_r = |F_{or}| - |sF_{cr}(a_1 \cdots a_n)|$.

Equation (9) is the full-matrix least-squares equation and may also be expressed as

$$\underline{\underline{M}}\ \underline{X} = \underline{Y}$$

where

$$M_{ij} = \sum_r \omega_r (\partial |sF_{cr}|/\partial p_i)(\partial |sF_{cr}|/\partial p_j)$$

$$X_i = \Delta p_i$$

and

$$Y_j = \sum_r \omega_r (\partial |sF_{cr}|/\partial p_j)\Delta F.$$

The elements of matrices $\underline{\underline{M}}$ and $\underline{Y}$ can be calculated and hence the shifts can be obtained from

$$\underline{X} = \underline{\underline{M}}^{-1}\underline{Y}.$$

When these shifts are applied to the initial parameters the result is an improved, but still approximate, set of parameters. These may then be used to repeat the process until successive cycles produce no further shifts. Multiple cycles are required because of the neglect of higher order terms in the Taylor series.

The matrix $\underline{\underline{M}}$ is a square matrix of order n where n is the number of variables. Since $\underline{\underline{M}}$ is also symmetric the number of unique elements which must be calculated and stored in the computer is $n(n+1)/2$. Since this number increases quite rapidly with n, the amount of computation time and memory space also increase significantly as larger structures are examined. Therefore, methods of approximating $\underline{\underline{M}}$ have been suggested[52] as a means of decreasing the computational

requirements for structural refinement.

An examination of the elements of $\underline{\underline{M}}$ shows that the diagonal elements are sums of squares and as more terms are accumulated these sums will become progressively larger. The off-diagonal elements, on the other hand, are sums of products which may be either positive or negative and as more terms are accumulated these sums could reasonably be expected to be smaller than those on the diagonal. If the parameters p_i and p_j are correlated in any way, however, the contributing terms to M_{ij} will not cancel in a random fashion and this element will be significantly different from zero. This is the case for terms correlating the scale factor with the thermal parameters and also for terms correlating parameters of a given atom, becoming especially important if the interaxial angles of the unit cell differ significantly from 90°.

The most commonly used approximation to $\underline{\underline{M}}$, therefore, is the block-diagonal matrix in which all off-diagonal elements are neglected except those corresponding to the different parameters associated with the same atom, thus forming 4x4 and 9x9 blocks for isotropic and anisotropic atoms, respectively. In order to account for the interaction between the scale factor and temperature factors, a common approach has been to include a 2x2 block in the matrix corresponding to the scale factor and overall temperature factor.

This and other block-matrix approaches, however, suffer

from overshifting of the parameters, especially in the early stages of refinement. The overshifting is caused by the omission of many important interactions when neglecting the off-diagonal elements of the full-matrix. Damping factors have to be applied to the calculated shifts in order for these methods to converge.

In ALLS, however, a somewhat different approach is used; each atomic block includes the row and column elements associated with the scale factor, thus forming 5x5 and 10x10 matrices. In this way many of the terms which are nonzero but are neglected in the other methods are now retained in the matrix and the parameters in different blocks are correlated to a common scale factor. No overall temperature factor is necessary to correlate the scale and temperature factors and, most significantly, no damping factors are needed.

Since each block contains the scale factor as a variable, a different scale factor shift is calculated for each atom. The total shift is then calculated as the weighted average:

$$\Delta s = \sum_i Z_i \Delta s_i / \sum_i Z_i \qquad (10)$$

where Z_i is the atomic number of atom i.

Sharpened Fourier Coefficients In the early stages of solving a structure, electron-density maps are calculated by

$$\rho(x,y,z) = \Sigma F_{hkl} \exp[-2\pi i(hx + ky + lz)]$$

and atoms are located by finding the peaks on these maps. Each F_{hkl} is a function of the scattering factors, f_i, as shown in Equations (3) and (4). If the atoms all had their scattering power concentrated at the nucleus and scattered as point atoms then f_i would be a constant, equal to the atomic number Z_i. For real atoms, however, f_i decreases with increasing θ and the resulting decrease in F_{hkl} at higher angles causes a broadening of peaks on the electron-density map. For small atoms this loss of resolution makes their peaks difficult to distinguish from background noise. If the F_{hkl}'s are multiplied by the factor $\Sigma Z_i / \Sigma f_i$, where Z_i is the atomic number and f_i is the scattering factor of atom i, then they will more closely resemble scattering from point atoms. To simplify the computations, ALLS uses the factor Z_1/f_1, the atomic number and scattering factor of the heaviest atom in the structure, as the sharpening factor and generates a sharpened data set for the electron-density map calculation.

Secondary Extinction Refinement The following equations, derived by Coppens and Hamilton,[53] are used when a secondary extinction parameter is included in the refinement:

$$y = (1 + g\gamma F_c)^{-1/2} \quad (11)$$

$$F = sF_c y^{1/2} \quad (12)$$

$$\partial F/\partial s = y^{1/2}\partial(sF_c)/\partial s \tag{13}$$

$$\partial F/\partial p_i = 0.5y^{1/2}(y^2 - 1)\partial(sF_c)/\partial p_i \tag{14}$$

$$\partial F/\partial g = -0.25sF_c^3y^{5/2} \tag{15}$$

where g is an isotropic extinction parameter and

$$y = -\frac{2}{12.593}\,\frac{1 + \cos^4 2\theta}{1 + \cos^2 2\theta}\,\frac{\bar{T}}{\sin 2\theta}\,\frac{\lambda^3}{\bar{V}^2} \tag{16}$$

$\bar{T}$ is the absorption-weighted mean path length of the beam in the entire crystal and is approximated in the program by using the transmission factor, T (as calculated in the program TALABS), and calculating

$$\bar{T} = -\ln(1 - T)/\mu. \tag{17}$$

Program Description

The program can be divided into four major parts: data input, calculation of structure factors and derivatives, matrix inversion, and output of results. Input is divided between subroutines PRELIM and NEWKI. PRELIM reads in the control information, scattering factor tables, symmetry operations, and parameters for the trial structure. The parameters are stored in the separate arrays SP, AI, XYZ, and BETA for convenience in calculating structure factors and derivatives, and in the single array P for convenience in making the least-squares adjustments. If isotropic temperature factors are to be converted to anisotropic form, PRELIM also

computes for each atom

$$\beta_{11}{}_i = B_i a^{*2}/4$$

$$\beta_{12}{}_i = B_i a^* b^* \cos\gamma^*/4, \quad \text{etc.}$$

where the β's are the anisotropic temperature coefficients used in the refinement and a^*, b^*, γ^* etc. are reciprocal cell parameters.

Input is finished via subroutine NEWKI which reads the parameter selection integers and stores them in the array KI. NEWKI also counts the number of variables (NV) and calculates the number of elements in the least-squares matrix (NMV). If the option is used which allows different parameters to be refined in each cycle, this subroutine is called once for each cycle of refinement; otherwise, it is called only at the beginning of the program.

The program then enters LSQR which serves primarily as a control routine for the rest of the program. The dimension for the array AM, which contains the upper diagonal part of the least-squares matrix, is set equal to NMV when this subroutine is called; LSQR is called each time NEWKI is called. LSQR consists of a loop which calls INIT, DERIV, TERM, SMI, and OUTP as required for each cycle. INIT simply initializes the arrays AM and V as well as the terms used for R factor calculations to zero.

DERIV calculates the scaled structure factor, YC, for each reflection and stores in the array DV the derivatives of

YC with respect to all parameters, p. (The derivative $\partial sF/\partial s$, is stored with the derivatives for each atom.) The expressions for these quantities are summarized in Table 27, in which F is the magnitude of the structure factor, s is the scale factor, A and B are the real and imaginary components of the structure factor, and p is any individual atom parameter.

Table 27. General form of structure factor-derivative relations

	Centrosymmetric with origin at symmetry center	Noncentrosymmetric
(sF)	$2s\lvert A\rvert$	$s(A^2+B^2)^{1/2}$
$\partial(sF)/\partial s$	$(sF)/s$	$(sF)/s$
$\partial(sF)/\partial p$	$2s(\partial\lvert A\rvert/\partial p)$	$s(A^2+B^2)^{-1/2}$ $*[A\partial A/\partial p + B\partial B/\partial p]$

The expressions for A and B and their derivatives are summarized in Table 28. Here the subscripts i and j refer to the various atoms in the asymmetric unit and to the different equivalent positions, respectively. T_i, f_i and a_i are the isotropic temperature factor coefficient, scattering factor, and scattering factor multiplier, respectively, for atom i. The terms $\cos_{ij}$, $\sin_{ij}$ and $\exp_{ij}$ are the trigonometric contributions and the anisotropic temperature factor of atom i

Table 28. Algebraic Expressions for the Derivatives

	Isotropic temperature factor	Anisotropic temperature factor
A	$\sum_i f_i a_i \exp(-T_i\rho) \sum_j \cos_{ij}$	$\sum_i f_i a_i \sum_j \exp_{ij} \cos_{ij}$
B	$\sum_i f_i a_i \exp(-T_i\rho) \sum_j \sin_{ij}$	$\sum_i f_i a_i \sum_j \exp_{ij} \sin_{ij}$
$\partial A/\partial a_i$	$f_i \exp(-T_i\rho) \sum_j \cos_{ij}$	$f_i \sum_j \exp_{ij} \cos_{ij}$
$\partial B/\partial a_i$	$f_i \exp(-T_i\rho) \sum_j \sin_{ij}$	$f_i \sum_j \exp_{ij} \sin_{ij}$
$\partial A/\partial T_i$	$-\rho f_i a_i \exp(-T_i\rho) \sum_j \cos_{ij}$	- - - - - - - - - - - -
$\partial B/\partial T_i$	$-\rho f_i a_i \exp(-T_i\rho) \sum_j \sin_{ij}$	- - - - - - - - - - - -
$\partial A/\partial x_i$	$-2\pi f_i a_i \exp(-T_i\rho) \sum_j h_j \sin_{ij}$	$-2\pi f_i a_i \sum_j h_j \exp_{ij} \sin_{ij}$
$\partial B/\partial x_i$	$2\pi f_i a_i \exp(-T_i\rho) \sum_j h_j \cos_{ij}$	$2\pi f_i a_i \sum_j h_j \exp_{ij} \cos_{ij}$
$\partial A/\partial \beta_{12_i}$	- - - - - - - - - - - -	$-f_i a_i \sum_j (2hk)_j \exp_{ij} \cos_{ij}$
$\partial B/\partial \beta_{12_i}$	- - - - - - - - - - - -	$-f_i a_i \sum_j (2hk)_j \exp_{ij} \sin_{ij}$

in equivalent position j.

The program does the computation for each reflection in three steps. First the sums over j are accumulated. These are then converted into the derivatives of A and B with respect to the atomic parameters, and A and B are obtained. Finally, the scaled structure factor and its derivatives are computed. If a secondary extinction coefficient is being refined these derivatives are then modified according to Equations (11)-(15). The derivatives are then stored in array DV for convenience in later calculations.

The following sums are accumulated for use in calculating various R factors:

$$RNUM(I) = \Sigma||F_o| - |sF_c||$$

$$RDEN(I) = \Sigma|F_c|$$

$$WRNUM(I) = \Sigma\omega(F_o - sF_c)^2$$

$$WRDEN(I) = \Sigma\omega F_o^2$$

$$XRNUM = \Sigma|F_o^2 - sF_c^2|$$

$$XRDEN = \Sigma F_o^2$$

where the different values of I represent summations over all reflections and over those reflections in specific hkl zones and ranges of $\sin\theta/\lambda$.

The contribution OMEGA*(YO-YC)*DV(J) is added to each vector element, V(J). The contributions to the matrix elements are then calculated if necessary. After the first cycle, if the full-matrix is being used and the shift/error

ratios were all less than ten on the previous cycle, the matrix element calculations would be skipped unless requested. If the full-matrix option is being used then the term OMEGA*DV(J)*DV(K) is added to AM(J,K), the jk^{th} element of the matrix. If, however, the block-diagonal matrix option is selected, then the contribution to AM(J,K) is only calculated if parameters J and K apply to the same atom or one of them is the scale factor.

After DERIV has processed all the reflections, the program calls the subroutine TERM to calculate and print the various R factors:

$$R(I) = RNUM(I)/RDEN(I)$$

$$\text{weighted } R(I) = WRNUM(I)/WRDEN(I)$$

$$\text{based on intensities} \quad R = XRNUM/XRDEN$$

The next step is the inversion of the matrix. The inversion procedure used in subroutine SMI is described in detail elsewhere.[54] If the matrix has not been recalculated this step is bypassed. Before calling SMI the program checks whether any diagonal element equals zero, which would indicate a singular matrix. If a singularity is discovered either at this point or during the inversion process, the program will terminate after printing an appropriate diagnostic message. If the block-matrix is being used then each block is inverted by a separate call to SMI. Upon completion of this stage the original matrix in AM has been replaced by

the inverse matrix.

The calculations are then completed in subroutine OUTP. First the matrix multiplication is performed to obtain the parameter shifts, PD, and at the same time the diagonal elements of the matrix are stored in DIAG. The entire list of parameters is then printed showing the changes which were made and the estimated standard errors associated with these variables. The latter are calculated as SQRT(DIAG(J)* SQSIG(1)) and are stored in ERP for later use. (SQSIG(1) is $(D/(r-n))^{1/2}$ where D is defined by Equation (1), r is the number of observations and n is the number of variables.) The overall scale factor shift is calculated as shown in Equation (10). Then the shifted parameters are transferred to the arrays AI, XYZ, and BETA and the estimated errors are transferred to ERXYX and ERBETA.

As the parameters and their errors are listed, several additional numbers are printed to help interpret the results. For the positional parameters the shift and estimated error are converted from fractional coordinates to angstroms and printed immediately after the shift/error ratio. The thermal parameters and their estimated errors are converted from β's to U's and these results are also printed after the shift/error ratio. The U's are defined by the expression

$$\exp[-0.25(U_{11}a^{*2}h^2 + U_{22}b^{*2}k^2 + U_{33}c^{*2}l^2 + 2U_{12}a^*b^*hk + 2U_{13}a^*c^*hl + 2U_{23}b^*c^*kl)]$$

and the conversions are made as follows:

$$U_{11} = 4\beta_{11}/a^{*2}$$

$$U_{12} = 4\beta_{12}/a^{*}b^{*} \quad \text{etc.}$$

All of these numbers are printed only for convenience in interpreting the results and are not saved or used in any other part of the program.

If necessary, related positional and thermal parameters and atom multipliers may be adjusted using the RESETX, RESETB and RESETA subroutines. The new thermal parameters are then tested for the positive-definite form in the following way. For isotropic temperature factors:

$$B_i \geq 0$$

For anisotropic temperature factors:

$$\beta_{11} \geq 0, \ \beta_{22} \geq 0, \ \beta_{33} \geq 0$$

$$\begin{vmatrix} \beta_{11} & \beta_{12} \\ \beta_{21} & \beta_{22} \end{vmatrix} \geq 0, \quad \begin{vmatrix} \beta_{11} & \beta_{13} \\ \beta_{31} & \beta_{33} \end{vmatrix} \geq 0, \quad \begin{vmatrix} \beta_{22} & \beta_{23} \\ \beta_{32} & \beta_{33} \end{vmatrix} \geq 0$$

$$\begin{vmatrix} \beta_{11} & \beta_{12} & \beta_{13} \\ \beta_{21} & \beta_{22} & \beta_{23} \\ \beta_{31} & \beta_{32} & \beta_{33} \end{vmatrix} \geq 0.$$

Failure of any of these tests means that the coefficients do not represent physical reality, in which case an appropriate message is printed describing the problem.

Upon completion of this test the program writes out the new parameters on a disk file which may serve as input for future jobs. If the job is in the final cycle these parameters are also punched on cards at the user's request.

Evaluation

Since this program was first developed it has been used successfully in the refinement of several structures. The new block-diagonal (B-D) method has proven to be a simplified and effective means of decreasing the cost of solving intermediate size structures (20-50 atoms) and making possible the refinement of larger structures (90 atoms or more). In order to compare the computational efficiency and rate of convergence of the B-D method with full-matrix refinement, several structures were refined by both methods. The computational advantage of the B-D method is due to the decreased number of matrix elements which must be calculated and stored within the computer and the subsequent decrease in the number of calculations involving the matrix, i.e., inverting the matrix and solving for parameter shifts. For the full-matrix the number of elements is given by $n(n+1)/2$, where n is the number of variables, and for the B-D matrix it is $15i + 55a$, where i is the number of isotropically refined atoms and a is the number of anisotropically refined atoms. A comparison of the two methods is provided in Table 29.

Table 29. Comparison of matrix size for full and block-diagonal matrices

Number of atoms	Number of matrix elements			
	Isotropic		Anisotropic	
	Full	Block	Full	Block
10	861	150	4186	550
20	3331	300	16471	1100
30	7381	450	36856	1650
50	20301	750	101926	2750
90	65341	1350	329266	4950

In order to determine how much computation time is saved by using the B-D method, a series of test runs was made using all 54 nonhydrogen atoms in $2Ni(C_8H_9O_2N_2)_2 \cdot 2H_2O$. By including all 54 atoms in every run the number of structure factor and derivative calculations remained constant and the changes in execution time were entirely due to changes in the number of matrix operations. Runs were made using both methods on identical sets of 10, 30, 50, 100, 200 and 300 variables and the execution times are plotted in Figure 10 as a function of the number of variables. From this plot it can be seen that the two methods are comparable for less than 50 variables but the B-D method is considerably faster for anything over 100 variables which is equivalent to 11 anisotropic atoms.

Because of the neglect of interatomic correlation, B-D methods converge more slowly than full-matrix refinement so more cycles are required. If significantly more cycles are required, then the total time spent in refining the structure

Figure 10. Execution time vs. number of variables for full and B-D matrix refinement. In each run one cycle of refinement was performed. All 54 non-hydrogen atoms in $2Ni(C_8H_9O_2N_2)_2 \cdot 2H_2O$ were included and 5957 reflections were used. The calculations were done on a CDC 7600/6600 computer system.

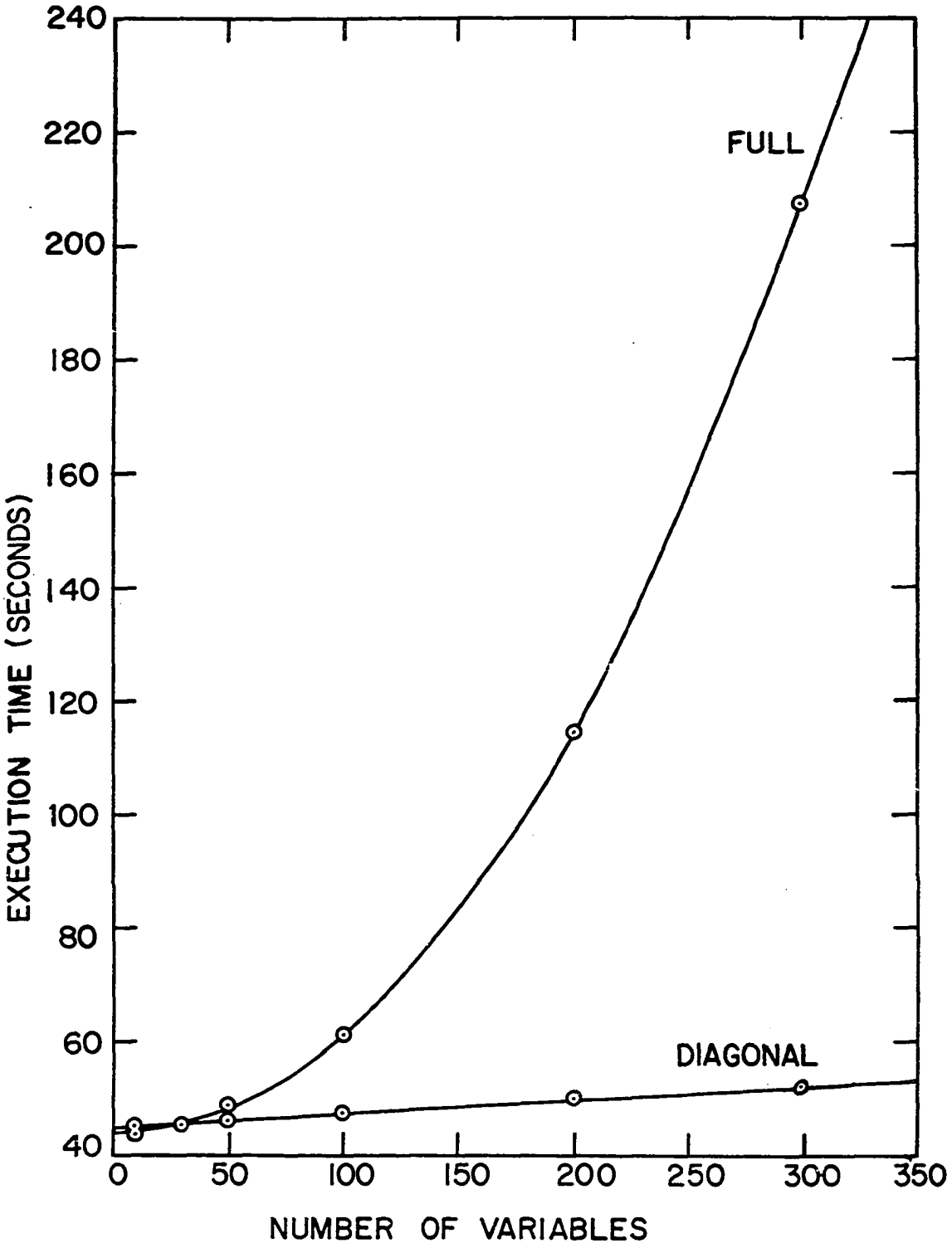
240
220
200
180
160
140
120
100
80
60
40
EXECUTION TIME (SECONDS)
FULL
DIAGONAL
0
50
100
150
200
250
300
350
NUMBER OF VARIABLES

by a B-D method could become greater than that for the full-matrix. To test this aspect of the program, parallel refinements were carried out on the $W(CO)(CSC_6H_5)(C_5H_5)(P(C_6H_5)_3)$ structure. All 35 nonhydrogen atoms were located before refinement began and the progress of the refinement was followed by comparing the conventional residual indices as shown in Table 30. From this table it can be seen that the B-D approximation worked as well as the full-matrix until thermal parameters were varied and even then only three cycles of B-D refinement were required for each two cycles of full-matrix refinement.

The combined effect of using a smaller portion of the computer system's memory and occupying that memory for a shorter period of time makes the B-D method highly economical. However, there are also potential disadvantages. As mentioned above, the neglect of correlation among interatomic terms can cause very slow convergence in the final cycles of refinement and can often cause the refinement to level off before the best solution is reached. For example, when the B-D method was tested on the α-calcium formate structure the R factor converged very slowly from 11.5 to 9.5 but in a single cycle of full-matrix refinement the R factor went from 9.5 to 6.2. In general, to obtain the best possible structure a final cycle of full-matrix refinement should be executed where feasible. (The final cycle of full-matrix

Table 30. Comparison of refinement by full-matrix and block-diagonal matrix techniques

Results are for the compound $W(CO)CSC_6H_5)(C_5H_5)(P(C_6H_5)_3)$. All 35 atoms were located before refinement began. Cycle #0 is the initial structure. Parameters refined in each cycle were: 1-scale factor and W position; 2,3 and 4-scale factor and all positions; 5,6 and 7-scale factor, positions and isotropic thermal parameters; 8,9-scale factor, positions and anisotropic thermal parameters.

Cycle	R factor	
#	Block	Full
0	20.3	20.3
1	12.7	12.7
2	11.3	11.3
3	11.1	11.1
4	11.1	11.1
5	9.9	8.3
6	8.5	8.2
7	8.2	8.2
8	7.2	7.1
9	7.1	7.0

refinement is also required in order to create a data set for the program ORFFE in which distances and angles and their estimated standard deviations are calculated.)

The reuse of the least-squares matrix on successive cycles has also proven to be a successful method for decreasing computation time when using the full-matrix. In each cycle after the first, time is saved by not recalculating the matrix elements and by not inverting the matrix. If the user wishes to recalculate the matrix in each cycle, this option must be overridden by setting a control variable on input; however, this has never been found to be necessary.

Another advantage of this program is the dynamic allocation of memory for the array containing the matrix elements. Standard FORTRAN requires fixed dimensions for all arrays. In the case of the least-squares matrix, if the array is given too small a dimension then large structures will not fit the program. On the other hand, if the array is given a very large dimension then a large amount of core memory is allocated to the program which would cause unnecessarily high cost and slow turn-around time for small structures. The solution to this in the past has been to compile several versions of the same program to handle structures of various sizes. ALLS, however, uses the GTMAIN subroutine available at the ISU Computation Center and allocates exactly the amount of memory required for the array as the program exe-

cutes. Thus only one program is required to handle any size problem. (The inclusion of full-matrix, B-D matrix and secondary extinction refinement in one program, plus the use of dynamic memory allocation, enables ALLS to replace twelve programs which were formerly used for refinement.)

In conclusion, a new block-diagonal matrix approximation has been shown to be a valid and efficient method of crystallographic refinement and has been included in a highly generalized least-squares refinement program. Reuse of the least-squares matrix, optional truncation of the data set, and dynamic memory allocation are other major features of this program which make it more efficient and more generally applicable than other refinement programs.

BIBLIOGRAPHY

1. W. J. Rohrbaugh and R. A. Jacobson, J. Agric. Food Chem., 24, 713 (1976).

2. W. J. Rohrbaugh and R. A. Jacobson, J. Agric. Food Chem., 25, 588 (1977).

3. R. A. Jacobson, J. Appl. Crystallogr., 9, 115 (1976).

4. F. Takusagawa, Iowa State University, Ames, Iowa, private communication, 1975.

5. W. J. Rohrbaugh and R. A. Jacobson, Inorg. Chem., 13, 2535 (1974).

6. E. R. Howells, D. C. Phillips and D. Rogers, Acta Crystallogr., 3, 210 (1950).

7. S. L. Lawton and R. A. Jacobson, Inorg. Chem., 1, 2124 (1968).

8. W. R. Busing, K. O. Martin and H. A. Levy, "ORFLS, A Fortran Crystallographic Least Squares Program", U. S. Atomic Energy Commission Report ORNL-TM-305, Oak Ridge National Laboratory, Oak Ridge, Tennessee, 1962.

9. C. A. Hubbard, C. O. Quicksall and R. A. Jacobson, "The Fast Fourier Algorithm and Programs ALFF, ALFFDP, ALFFPROJ, ALFFT, and FRIEDEL", U. S. Atomic Energy Commission Report IS-2625, Iowa State University and Institute for Atomic Research, Ames, Iowa, 1971.

10. H. P. Hanson, F. Herman, J. D. Lea, and S. Skillman, Acta Crystallogr., 17, 1040 (1960).

11. D. H. Templeton, in "International Tables for X-ray Crystallography," Vol. III, Table 3.3.2c, The Kynoch Press, Birmingham, England, 1962, pp 215-216.

12. R. F. Stewart, E. R. Davidson and W. T. Simpson, J. Chem. Phys., 42, 3175 (1965).

13. W. R. Busing, K. O. Martin and H. A. Levy, "ORFEE, A Fortran Crystallographic Function and Error Program", U. S. Atomic Energy Commission Report ORNL-TM-306, Oak Ridge National Laboratory, Oak Ridge, Tennessee, 1964.

14. C. A. Johnson, "ORTEP II: A Fortran Thermal-Ellipsoid Plot Program for Crystal Structure Illustrations", U. S.

Atomic Energy Commission Report ORNL-3794 (Second Revision with Supplemental Instructions), Oak Ridge National Laboratory, Oak Ridge, Tennessee, 1971.

15. J. A. Pople and D. L. Beveridge, "Approximate Molecular Orbital Theory", McGraw-Hill, New York, 1970.

16. R. M. Krupka, Can. J. Biochem., 42, 677 (1964).

17. C. Chothia and P. Pauling, Nature 223, 919 (1969).

18. P. M. Hollingworth, T. R. Fukuto and R. L. Metcalf, J. Agric. Food Chem., 15, 235 (1967).

19. R. D. O'Brien, J. Agric. Food Chem., 11, 163 (1963).

20. M. Eto, "Organophosphorus Insecticides: Organic and Biological Chemistry," CRC Press, Cleveland, Ohio, 1974.

21. R. G. Baughman and R. A. Jacobson, J. Agric. Food Chem., 23, 811 (1975).

22. R. G. Baughman and R. A. Jacobson, J. Agric. Food Chem., 24, 1036 (1976).

23. R. G. Baughman and R. A. Jacobson, J. Agric. Food Chem., 26, 403 (1978).

24. R. G. Baughman, D. A. Eckey and R. A. Jacobson, J. Agric. Food Chem., 26, 398 (1978).

25. R. G. Baughman and R. A. Jacobson, J. Agric. Food Chem., 25, 582 (1977).

26. R. G. Baughman and R. A. Jacobson, J. Agric. Food Chem., 26, 576 (1978).

27. D. E. Beckman and R. A. Jacobson, J. Agric. Food Chem., in press.

28. D. W. Osborne, Dow Chemical Company, Midland, Mi., private communication, 1979.

29. P. M. Main, M. M. Woolfson, and G. Germain, "MULTAN: A Computer Program for the Automatic Determination of Crystal Structures", Department of Physics, University of York, York, England, 1971.

30. F. Takusagawa, Iowa State University, Ames, Iowa, private communication, 1975.

31. J. Karle and I. L. Karle, Acta Crystallogr., 21 849 (1966).

32. V. M. Clark, D. W. Hutchinson, A. I. Kirby and S. G. Warren, Angew. Chem., 76, 704 (1964).

33. L. Pauling, "Nature of the Chemical Bond", Cornell University Press, Ithaca, N. Y., 1960.

34. H. O. Michel, Fed. Proc., 14, 255 (1955).

35. H. S. Aaron, H. O. Michel, B. Witten and J. I. Miller, J. Am. Chem. Soc., 80, 456 (1958).

36. G. Hilgetag and G. Lehmann, J, Prakt. Chem., 8, 224 (1959).

37. A. J. J. Ooms and H. L. Boter, Biochem. Pharmacol., 14, 1839 (1965).

38. T. R. Fukuto and R. L. Metcalf, J. Econ. Entomol., 52, 739 (1959).

39. H. L. Boter and C. Van Dijk, Biochem. Pharmacol., 18, 2403 (1969).

40. T. R. Fukuto and R. Allahyari, University of California, Riverside, California, private communication, 1978.

41. R. Allahyari, P. W. Lee, G. Y. H. Lin, R. M. Wing and T. R. Fukuto, J. Agric. Food Chem., 25, 471 (1977).

42. R. A. Jacobson and D. E. Beckman, Acta Crystallogr., in press.

43. R. L. Lapp and R. A. Jacobson, "ALLS: A Generalized Crystallographic Least Squares Program," USDOE Report, in preparation, 1979.

44. I. Nitta, X-Rays, 5, 37 (1948).

45. C. J. H. Schutte and K. Buijs, Spectrochim. Acta, 20, 187 (1964).

46. J. D. Donaldson, J. F. Knifton and S. D. Ross, Spectrochim. Acta, 20, 847 (1964).

47. C. Comel and B. F. Mentzen, J. Solid State Chem., 9, 210 (1974).

48. R. W. Vaughan, California Institute of Technology, Pasadena, California, private communication, 1976.

49. C. G. Darwin, Phil. Mag., 43, 800 (1922).

50. N. Burger, H. Fuess and S. A. Mason, Acta Crystallogr., B33, 1968 (1978).

51. K. K. Taylor and G. J. B. Williams, ACA Summer Meeting, 1977.

52. R. A. Sparks, in "Computing Methods and the Phase Problem in X-Ray Crystal Analysis," Pergamon Press, New York, 1961, pp 170-187.

53. P. Coppens and W. C. Hamilton, Acta Crystallogr., A26, 71 (1971).

54. W. R. Busing and H. A. Levy, "A Procedure for Inverting Large Symmetric Matrices," Comm. ACM, 5, 445 (1962).

55. D. Rogers, in "Computing Methods in Crystallography," Pergamon Press, Oxford, England, 1965, pp 117-132.

56. A. J. C. Wilson, Acta Crystallogr., 2, 318 (1949).

57. J. H. Campbell, G. F. Covert and B. J. Helland, USERDA Report IS-3339, Ames, Iowa, 1976.

58. D. G. Adolphson and J. D. Corbett, Inorg. Chem., 15, 1820 (1976).

59. R. L. Daake and J. D. Corbett, Inorg. Chem., 16, 2029 (1977).

60. A. W. Struss and J. D. Corbett, Inorg. Chem., 16, 360 (1977).

61. P. W. DeHaven, Ph. D. Dissertation, Iowa State University, Ames, Iowa, 1977.

ACKNOWLEDGEMENTS

The author would like to express his appreciation to Dr. R. A. Jacobson for his invaluable guidance and inspiration in the course of this research, to James Benson for keeping the laboratory instruments running smoothly, to Barbara Helland for her assistance in the development of the computer programs, and to all the members of the x-ray research group whose friendship and assistance helped make graduate school such an enjoyable experience.

The author would also like to express special thanks to his parents without whom none of this would have been possible.

APPENDIX A: STATISTICAL INTERPRETATION OF INTENSITY DATA

Introduction

One of the major efforts in this group in recent years has been toward the development of a highly efficient routine for the collection and refinement of x-ray single crystal diffraction data. Refinement of the data begins with interpretation of the intensity data and several statistical tests have been derived which are often helpful in the preliminary interpretation. Two of these are the Howells, Phillips and Rogers (HPR) test[55] and the Wilson plot.

The HPR test is based on the effect of symmetry on the distribution of intensities. Centric structures are characterized by considerable fractions of both faint and accidentally absent reflections and also conspicuously strong reflections. Acentric structures, on the other hand, are noteworthy for the "sameness" of their intensities. Expressions have been derived for the distribution of intensities in each type of symmetry and by comparison of these theoretical distributions with that observed for an experimental crystal one can obtain some evidence as to the presence or absence of a center of symmetry in the crystal structure. This is especially helpful when such a distinction cannot be made on the basis of observed extinction conditions.

The Wilson plot is a convenient method for obtaining a

good estimate of the scale factor required to place the observed structure factors on an absolute scale. It is based on the fact that the average intensity depends only on what is in the cell and not where it is.

Mathematical Background

Howells, Phillips and Rogers test The most general definition of the structure factor is

$$F(\vec{h}) = \sum_i f_i \exp(2\pi i \vec{h}\cdot\vec{r}_i) \qquad (A1)$$

where f_i is the atomic scattering factor of the atom located at $\vec{r}_i$. If the atoms are placed at random locations then the structure factor is a sum of random vectors and may be treated as an example of a random walk problem. Any symmetry in the cell will impose some constraints on the individual atomic contributions and thus upon the whole reciprocal lattice. In particular, if a center of symmetry is present the vectors will pair off such that their resultant is real and so is $F(\vec{h})$.

$$F(\vec{h}) = 2\sum_i f_i \cos(2\pi \vec{h}\cdot\vec{r}_i) \qquad (A2)$$

This may be treated as a one-dimensional random walk along the real axis and expressions have been published by several workers for the probability of finding any value of $|F|$. Wilson[56] derived the expression most commonly used,

$$(\bar{1})\ P(F)dF = (2/\pi S)^{1/2}\exp(-F^2/2S)dF \qquad (A3)$$

which can be re-expressed in terms of the intensity as

$$_{(\bar{1})}P(I)dI = (2\pi SI)^{-1/2}\exp(-I/2S)\,dI. \qquad (A4)$$

In these equations S is defined by $S = \Sigma f_i^2$ and it can be shown by Equation (A4) that $S = \langle I \rangle$.

In the absence of symmetry, $F(\vec{h})$, defined by Equation (A1), is complex and may be treated as a two-dimensional random walk problem in the complex plane. Both the real and imaginary components conform to Equation (A3) but, so long as they are uncorrelated, they combine to give

$$_{(1)}P(F)dF = (2|F|/S)\exp(-F^2/S)\,dF \qquad (A5)$$

and

$$_{(1)}P(I)dI = S^{-1}\exp(-I/S)\,dI \qquad (A6)$$

If each intensity is expressed in terms of its local average, $z = I/\langle I \rangle$, we can re-express Equations (A6) and (A4) as

$$_{(1)}P(z) = \exp(-z) \qquad (A7)$$

$$_{(\bar{1})}P(z) = (2\pi z)^{-1/2}\exp(-z/2) \qquad (A8)$$

Early attempts to use the P(z) frequency plots for distinguishing the two distributions showed them to be unduly susceptible to small sample errors. The cumulative distributions

$$N(z) = \int_0^z P(z)\,dz$$

have been found to be preferable. These are

$$_{(1)}N(z) = 1 - \exp(-z)$$

and

$$_{(\bar{1})}N(z) = \mathrm{erf}(z/2)^{1/2}.$$

Wilson Plot For a unit cell with n atoms it has been shown that the theoretical average intensity is given by,

$$\langle I \rangle = \Sigma f_i^2 \qquad (A9)$$

i.e., the average intensity depends only on what is in the cell and not where it is.

Ideally, the scaling factor required to place the observed intensities on an absolute scale would be the ratio of $\langle I_{abs} \rangle$ to $\langle I_{obs} \rangle$. However, the f_i's are functions of $\sin\theta/\lambda$ so the problem is not so simple. Furthermore, in real atoms the f's required are those which include thermal motion, i.e.

$$\langle I_{abs} \rangle = \Sigma f_i^2 \exp(-2B\sin^2\theta/\lambda^2) \qquad (A10)$$

where the B must also be determined. If B is assumed to be the same for all atoms then the exponential term can be factored out

$$\langle I_{abs} \rangle = \exp(-2B\sin^2\theta/\lambda^2)\Sigma f_i^2 \; . \qquad (A11)$$

Now if

$$\langle I_{obs} \rangle = C\langle I_{abs} \rangle \qquad (A12)$$

$$\langle I_{obs} \rangle = C\exp(-2B\sin^2\theta/\lambda^2)\Sigma f_i^2 \qquad (A13)$$

$$\langle I_{obs} \rangle / \Sigma f_i^2 = C\exp(-2B\sin^2\theta/\lambda^2) \qquad (A14)$$

and taking the logarithms of both sides,

$$\ln(\langle I_{obs} \rangle / \Sigma f_i^2) = \ln C - 2B\sin^2\theta/\lambda^2 \; . \qquad (A15)$$

If the left side of Equation (A15) is plotted against $\sin^2\theta/\lambda^2$ then a straight line should be obtained with a slope

of -2B and the scale factor required to place the observed structure factors on an absolute scale is

$$k = C^{-1/2}$$

where

$$|F_{abs}| = k|F_{obs}|.$$

In practice the method used is to divide the data into concentric shells of $\sin\theta/\lambda$ such that the f's can be considered constant within each shell. The average intensity in each shell is then calculated as is the left side of Equation (A15).

Program Description

The Wilson plot and the HPR test have both been programmed as integral parts of the data collection algorithm used in this Laboratory. The programming language used is a subset of PL/1, ALECS,[57] developed in this Laboratory.

The sums required to calculate the local average intensities are accumulated as the data are collected. All data with $\sin^2\theta/\lambda^2$ in the range 0.00497 to 0.29092 are divided into seven shells in equal increments of $\sin^2\theta/\lambda^2$. Reflections falling outside these limits and those with negative net intensities are not included. Within each shell a summation over all the intensities is accumulated and each sum is stored in one element of the array AVI(I). The array M(I) stores the number of reflections in each shell.

Since the individual intensities are required later, the reflection data are also stored on disk. Because of the limited amount of disk space available in the minicomputer, the data are stored in compressed form by packing h, k and l into a single word. Since a floating point number is stored as two words and an integer as one word, the structure factor is scaled up by 100 and stored as an integer. A third word is also stored which contains a digit between 1 and 7 corresponding to the shell in which the reflection is located. The data set is limited to 4000 reflections and when the available space is filled the program sets a flag so that no more reflections will be stored.

Upon completion of data collection the intensity summations and number of reflections in each shell are passed into subroutine HPR1. HPR1 asks if an HPR plot is desired and if so how many octants should be used. The number of octants required for a unique set of data should be entered. The program detects a change in octants by a change in the signs of the indices and stops when the appropriate number of octants has been used. The average intensity, $\langle I \rangle_x$, in each shell is then calculated and the distribution of intensities in each shell is determined. The array AN(I,J) is a 9x7 matrix used to accumulate the intensities as follows:

A reflection is read in and determined to belong in shell X. The quantity $z = I/\langle I \rangle_x$ is calculated where I is

the individual intensity and $\langle I \rangle_x$ is the average intensity of all the reflections in shell X. If M(X) is the number of reflections in shell X, then the quantity 1/M(X) is added to each AN(Y,X) for which z < Y/10.

After all the reflections have been read in and the distributions in each shell have been accumulated, these distributions are added together to get a total distribution

$$D(I) = \sum_K AN(I,K) * M(K)$$

and D(I) is then the cumulative distribution of intensities. Each term in this array is then compared to the theoretical values for centric symmetry, shown in Table 31, and if seven out of the nine values are greater than or equal to the theoretical centric values then the prediction of centric symmetry is made; otherwise, the program predicts acentric symmetry.

The program then prints a graph of N(z) vs. z showing the theoretical centric curve as +'s, the acentric curve as *'s and the observed curve as 0's. If an observed value exactly matches a theoretical value then only the 0 is printed. Figures 11 and 12 show sample output for centric and acentric structures, respectively.

After printing the graph the program asks if a Wilson plot is to be calculated. If so, then the program asks for the number of different elements in the crystal. For each element the program requests the atomic number and number of

Table 31. Theoretical cumulative intensity distributions, N(z), for centric and acentric symmetry

z	Centric	Acentric
0.1	0.2486	0.0952
0.2	0.3450	0.1813
0.3	0.4157	0.2592
0.4	0.4736	0.3297
0.5	0.5205	0.3935
0.6	0.5616	0.4519
0.7	0.5967	0.5034
0.8	0.6289	0.5507
0.9	0.6572	0.5934

```
TYPE Y FOR HPR PLOT?Y
NUMBER OF OCTANTS TO BE READ.?2


ALICE SAYS THE UNIT CELL IS     CENTRIC

WILSON RATIO=      .61285


PLOT OF N(Z) VALUES VERSUS Z
0 = CALCULATED VALUE
+ = CENTRIC VALUE
* = ACENTRIC VALUE
```

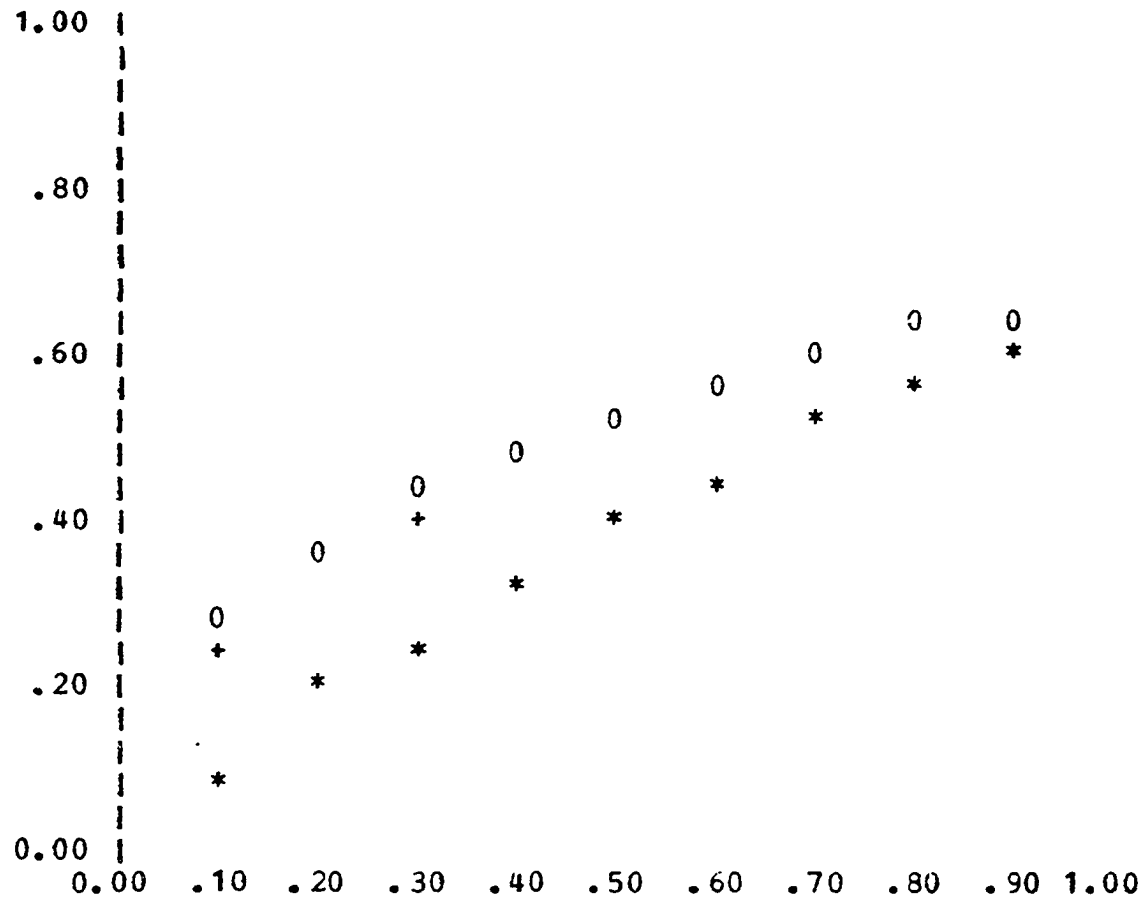

Figure 11. Sample output from HPR plot for a data set displaying centric symmetry

```
TYPE Y FOR HPR PLOT?Y
NUMBER OF OCTANTS TO BE READ.?2


ALICE SAYS THE UNIT CELL IS     ACENTRIC

WILSON RATIO=      .72311


PLOT OF N(Z) VALUES VERSUS Z
0 = CALCULATED VALUE
+ = CENTRIC VALUE
* = ACENTRIC VALUE
```

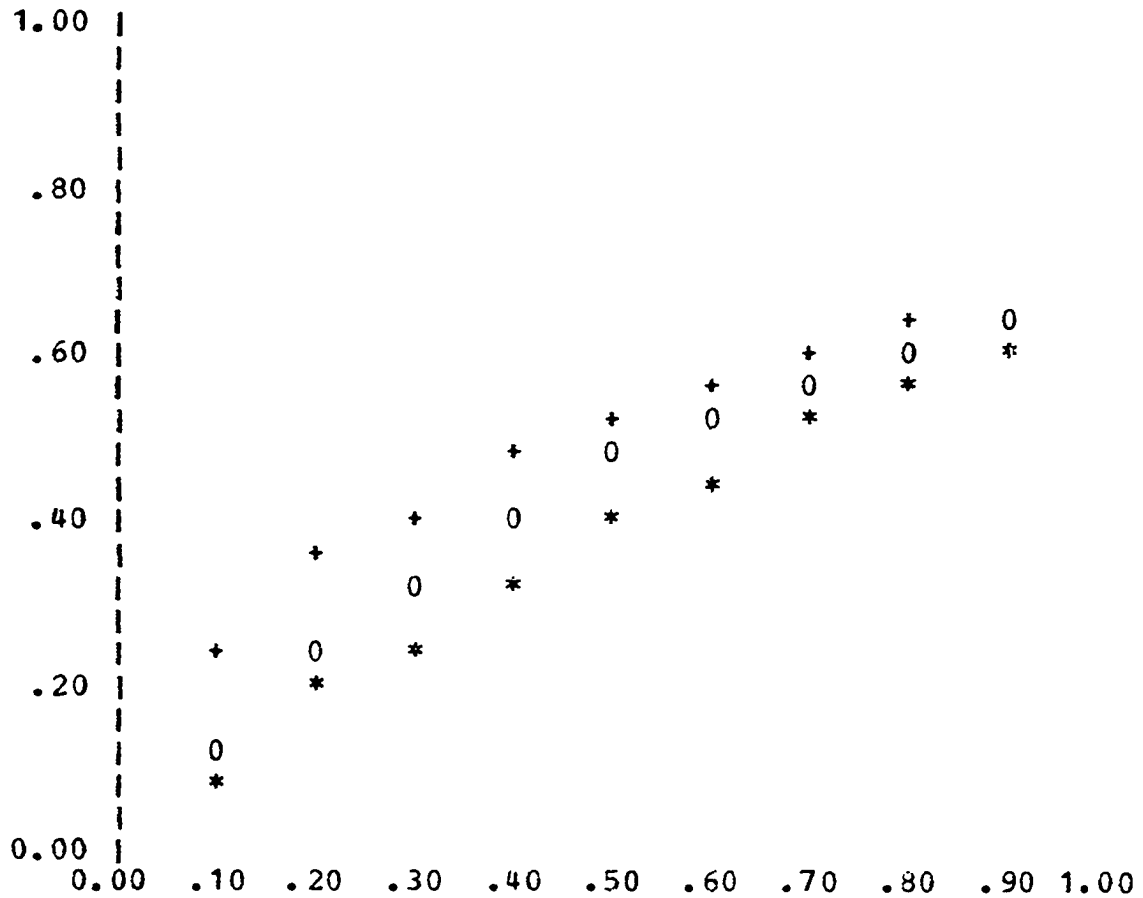

Figure 12. Sample output from HPR plot for a data set displaying acentric symmetry

atoms per unit cell. For each of the seven groups of reflections the left side of Equation (A15) is calculated as

$$\ln(\langle I\rangle_j / \Sigma_i N_i Z_i f_j)$$

where $\langle I\rangle_j$ is the average intensity in the j^{th} shell, N_i is the number of atoms of element i, Z_i is the atomic number of element i, and f_j is a unit scattering factor at an angle corresponding to the j^{th} shell of reflections. These f_j's were obtained by taking the scattering factor for oxygen at the $\sin\theta/\lambda$ values corresponding to the upper limits of the j shells and dividing by eight, the atomic number of oxygen. The scattering factor for any element is then approximated by multiplying these f_j's by the atomic number of the element. This approximation is made to reduce the space which would be required to store individual scattering factors for all the elements. The seven points are then plotted against $\sin^2\theta/\lambda^2$, again using the value at the upper limit of each shell, and the line of best fit is then determined by least-squares techniques. The temperature factor is determined from the slope of this line and the scale factor from the intercept and all of these numbers are printed. The output is completed with a graph showing the calculated points and the least-squares line. A sample of the input and output for the Wilson plot is shown in Figure 13.

```
WILSON PLOT? Y OR N?Y
NUMBER OF DIFFERENT ELEMENTS?6
FOR EACH ELEMENT GIVE: ATOMIC #,# OF ATOMS/CELL
       1?35?4
       2?17?8
       3?16?4
       4?15?4
       5?8?8
       6?6?52


SLOPE=  -0.6918780E01   TEMPERATURE FACTOR=      0.3459390E01
INTERCEPT=       0.5080674E00   SCALE FACTOR=    0.7756656E00
```

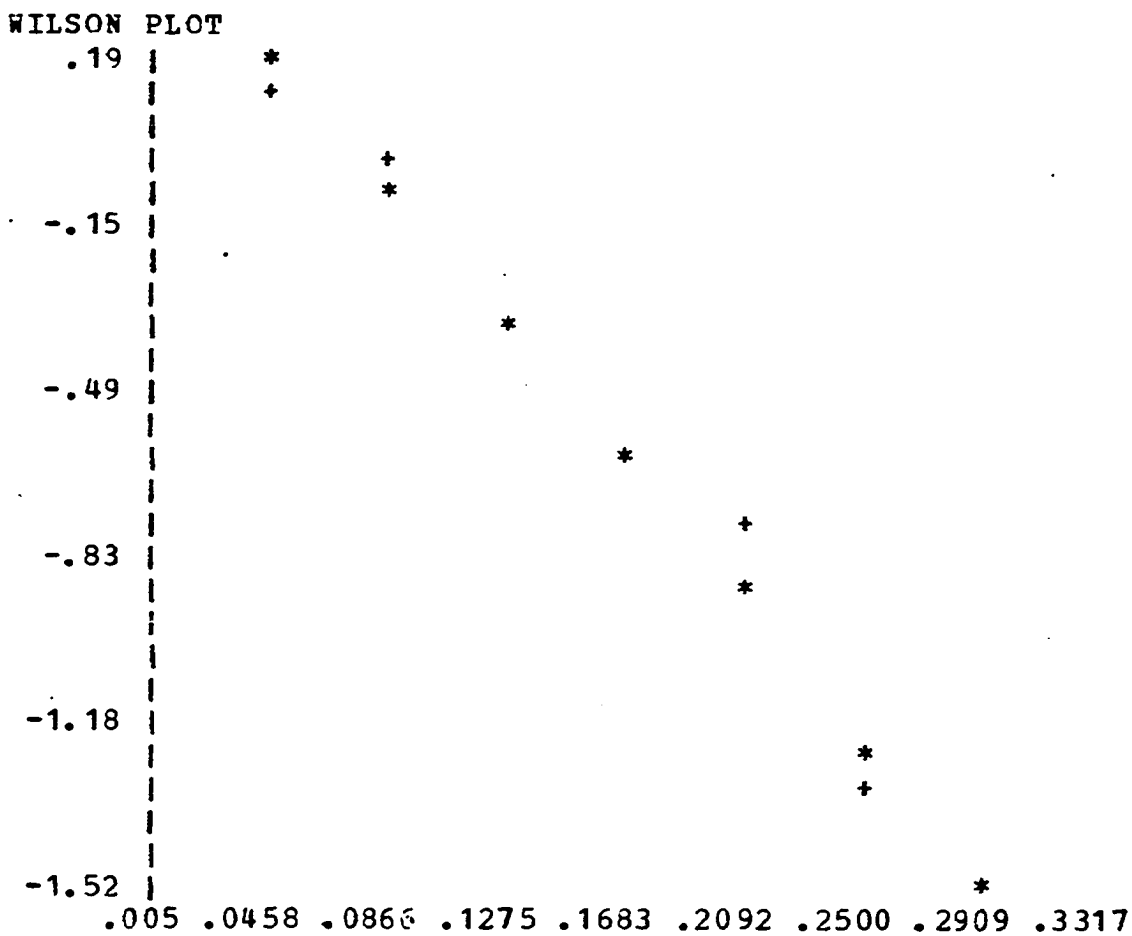

Figure 13. Sample listing of the input and output for the Wilson plot obtained using the leptophos data

Evaluation

The advantage of having the HPR and Wilson plots incorporated into the data collection procedure is primarily the rapid availability of the results. Immediately upon completion of data collection the user need only enter a single command to the computer to obtain the HPR plot and a minimal set of parameters to obtain a Wilson plot. This eliminates the time and effort, and inevitable mistakes, involved in preparing to run the equivalent programs in batch-mode after reducing the data at the Computer Center.

The HPR plot works quite well although some approximations were necessary to run in real-time mode. Ideally, the systematically extinct reflections should not be included in this test. However, since it is impossible to know which reflections are systematically extinct until data collection has progressed far enough to observe the extinctions, the program treats all reflections as symmetry allowed. This is not a serious problem for relatively low symmetry crystals but for centered space groups, where there are many extinct reflections, the low intensity reflections would be overweighted and the test would give erroneous results. A similar problem occurs if a crystal diffracts weakly so that there are many unobserved reflections. Since a large proportion of low intensity reflections is characteristic of centric symmetry, an HPR test may predict centric symmetry for

an acentric cell due to experimental and symmetry effects which cause a large number of such low intensities. In general, therefore, a prediction of centric symmetry cannot be taken as proof of a center of symmetry, but a prediction of acentric symmetry is very strong evidence that there is not a center of symmetry. The plots shown in Figures 11 and 12 were obtained from the data for leptophos and dimethoate, respectively. In each case the symmetry was correctly predicted.

The Wilson plot has been similarly successful in predicting scale factors although the approximation used for the scattering factors has been found to introduce a slight overestimate of the scale factor and underestimate of the temperature factor. Using data from a dimethoate crystal this program predicted k = 0.392 and B = 3.96 while a more sophisticated program including the exact scattering factors yielded k = 0.352 and B = 4.79. A comparison of the predicted scale factors with those obtained in the final cycle of refinement confirms a slight overestimate; 0.776 vs. 0.607 for leptophos, 0.391 vs. 0.371 for IPAT, and 0.248 vs. 0.124 for α-calcium formate. However, since k and B are only used as starting parameters to be refined in the least-squares procedure the results from this program are quite satisfactory. It should be pointed out that since the scale factor in the least-squares procedure is applied to the

F_{abs}'s rather than the F_{obs}'s, the reciprocal of k is used in the refinement program.

In conclusion the HPR and Wilson plots have been successfully integrated into a data collection algorithm and have been found to provide rapid and accurate statistical evaluations of the intensity data.

APPENDIX B: ZIRCONIUM BROMIDE HYDRIDES

Introduction

Corbett et al. have recently been involved in the development of methods to prepare metallic halides, i.e., halide salts which are metallike in their electrical conductivity. Two of these halides, ZrCl[58] and ZrBr,[59] were chosen for use in an investigation of the fundamental properties of potential hydrogen storage materials.[60] The ZrCl and ZrBr react reversibly with hydrogen to form the phases $ZrClH_{0.5}$, ZrClH, $ZrBrH_{0.5}$ and ZrBrH which are thermodynamically stable with respect to disproportionation into binary halides and hydrides. On the basis of the strong Zr-H interactions observed, Corbett has concluded that the compounds are hydridic or contain phases at least as hydridic as binary zirconium hydride. In order to better understand the Zr-H interaction it would be very helpful to know the positions of the hydrogen atoms in the hydrides and hemihydrides. The ZrCl and ZrBr structures have been investigated by x-ray diffraction analysis and both salts were found to be basically two-dimensional metals consisting of infinite double metal layers separated by double layers of halide. Therefore, a neutron diffraction investigation was initiated to locate the hydrogen atoms. Because of the negative scattering length and high degree of incoherent scattering by hydrogen, the

deuterides were also used for these investigations. Samples of $ZrBrH_{0.5}$, $ZrBrD_{0.5}$ and ZrBrD were kindly supplied by Struss and Corbett.

Experimental

The samples used for data collection consisted of powders contained in a thin-walled (∿5 mil) cylindrical aluminum sample holder 1 cm. in diameter and 4 cm. in height. The neutron diffraction data were collected at the 5MW Ames Laboratory Research Reactor (ALRR) on a two-axis diffractometer modified[61] for multiple-wavelength diffraction (λ_1 = 1Å, λ_2 = 2Å). Each data set was collected as follows:

$ZrBrH_{0.5}$ A series of 5 scans was run from 2θ = 16° to 2θ = 100° in increments of 0.2° 2θ. The data were averaged and a plot of the resulting averaged scan is shown in Figure 14. A series of three scans was run over the same range on the empty sample holder and the average of these three scans was subtracted from the data to correct for background.

$ZrBrD_{0.5}$ A series of 4 scans was run from 2θ = 8° to 2θ = 110° in increments of 0.2° 2θ. The data were averaged and a plot of the resulting averaged scan is shown in Figure 15.

ZrBrD Two scans were run from 2θ = 6° to

2θ = 110° in increments of 0.1° 2θ. The data were averaged and a plot of the resulting averaged scan is shown in Figure 16.

An additional three scans were made on the empty sample holder from 2θ = 16° to 2θ = 100° in increments of 0.2° 2θ and the data were averaged to produce a background correction for the second and third data sets. All of the averaged data sets are punched on computer cards for permanent storage.

Results

The original intention was to obtain reasonable starting models of the structures and then refine the parameters using the recently developed multiple-wavelength profile refinement algorithm.[61] It was first assumed that the ZrBr structure is not significantly altered by the addition of deuterium, so that the coordinates of Zr and Br are the same as in the non-deuterated species. Then, assuming that the deuterium occupies the interstitial sites within the Zr-Zr double layer, there are 0.5 octahedral and 1.0 tetrahedral sites available per ZrBr formula unit. Therefore, a model placing the deuterium in all the octahedral sites seemed reasonable for the hemideuteride and a model with deuterium occupying all the tetrahedral sites was selected for the deuteride. The cell constants, atomic coordinates and symmetry information for this model are included in Table 32. However, since powder

patterns based on these models, calculated with the program YCALC, differed significantly from the observed patterns, these models were discarded. A series of models was then tested by varying the proportion of deuterium in tetrahedral and octahedral sites but no model could be found to provide a match for the observed data. Indeed, no model was close enough to the correct structure for the refinement program to be used.

The interpretation of these data was made more difficult by lack of resolution and overlap of the two wavelength contributions. After the closing of the ALRR the ZrBrD sample was sent to the University of Missouri Reactor and a set of higher resolution data was obtained with monochromated neutrons (λ = 1.103 Å). These data were obtained via a single scan from 2θ = 3.0° to 2θ = 80° and are shown in Figure 17. With these data it was possible to index the reflections and determine more accurate cell parameters. The lattice constants for the hexagonal cell are a = 3.488 Å and c = 29.298 Å which yields a cell volume about 3% larger than for the nondeuterated species. A calculated pattern based on this cell matches the positions of the peaks in the neutron and x-ray diffraction data except for a difference of 0.2° 2θ for the 0,0,21 reflection which is weakly observed with x-rays but unobserved with neutrons.

An attempt was made to calculate a Patterson map using

estimated individual intensities from these data. However, the map yielded no useful information.

A comparison of the observed x-ray and neutron diffraction patterns should yield some information. In particular, the 012 reflection at 21.49° 2θ is observed with x-rays but not with neutrons while just the reverse is true for the 013 reflection at 22.03° 2θ. This would suggest that the deuterium atoms are concentrated along these planes and should provide a clue to the positions if the indexing is correct. In general, the agreement between the calculated and observed positions of diffraction peaks for both x-ray and neutron data indicates that the indexing is reasonable.

The failure to obtain a good starting model is strong evidence that the ZrBr structure has changed significantly, contradicting one of our basic assumptions. Further work on the structures of these hydrides should be done with x-ray data in order to more precisely determine the positions of the Zr and Br atoms. With this information available it should be possible to interpret the neutron data and obtain the hydrogen positions.

Table 32. Parameters used in the trial structures of $ZrBrD_{0.5}$ and ZrBrD

space group	$R\bar{3}m$			
equivalent positions	(0,0,0; 1/3,2/3,2/3; 2/3,1/3,1/3) +			
	0,0,z, 0,0,-z			
unit cell parameters	a = 3.5031 Å			
	c = 28.071 Å			
atomic positions	Zr	0.0	0.0	0.2902
	Br	0.0	0.0	0.3917
octahedral	D	0.0	0.0	0.5000
tetrahedral	D	0.0	0.0	0.1390

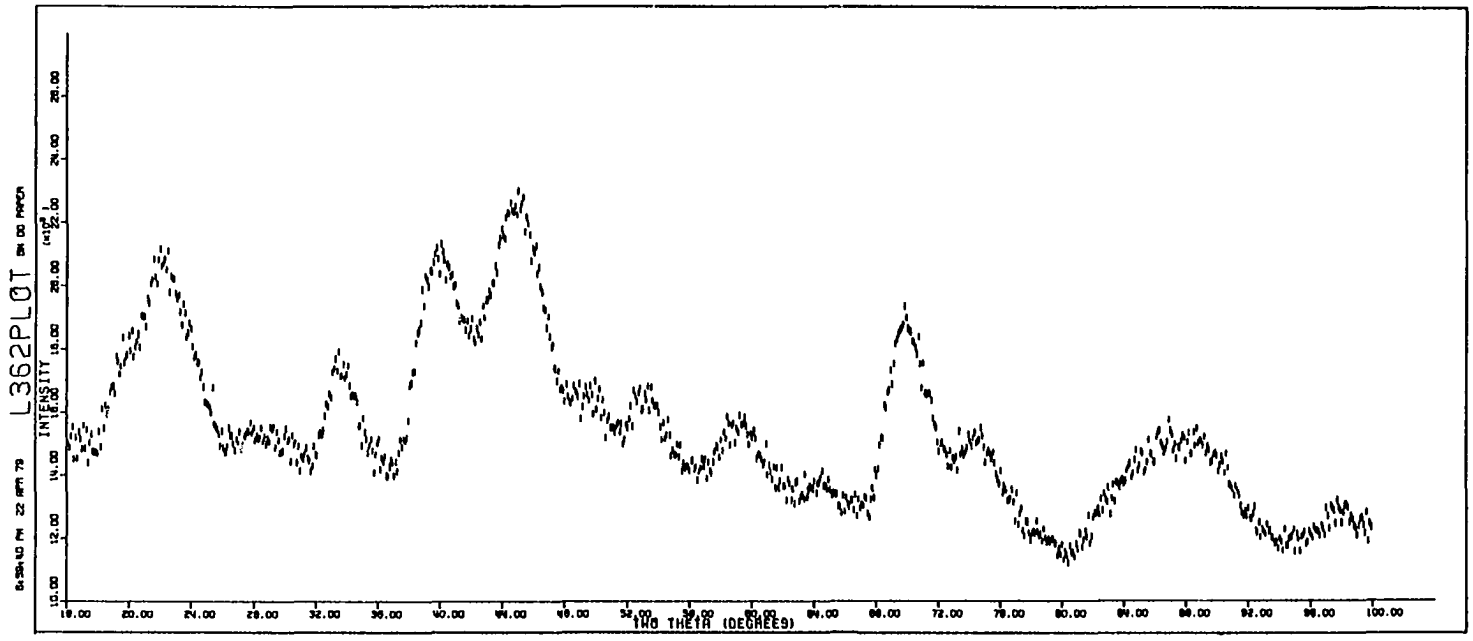

Figure 14. Neutron diffraction pattern of $ZrBrH_{0.5}$ obtained from the multiple wavelength diffractometer at ALRR

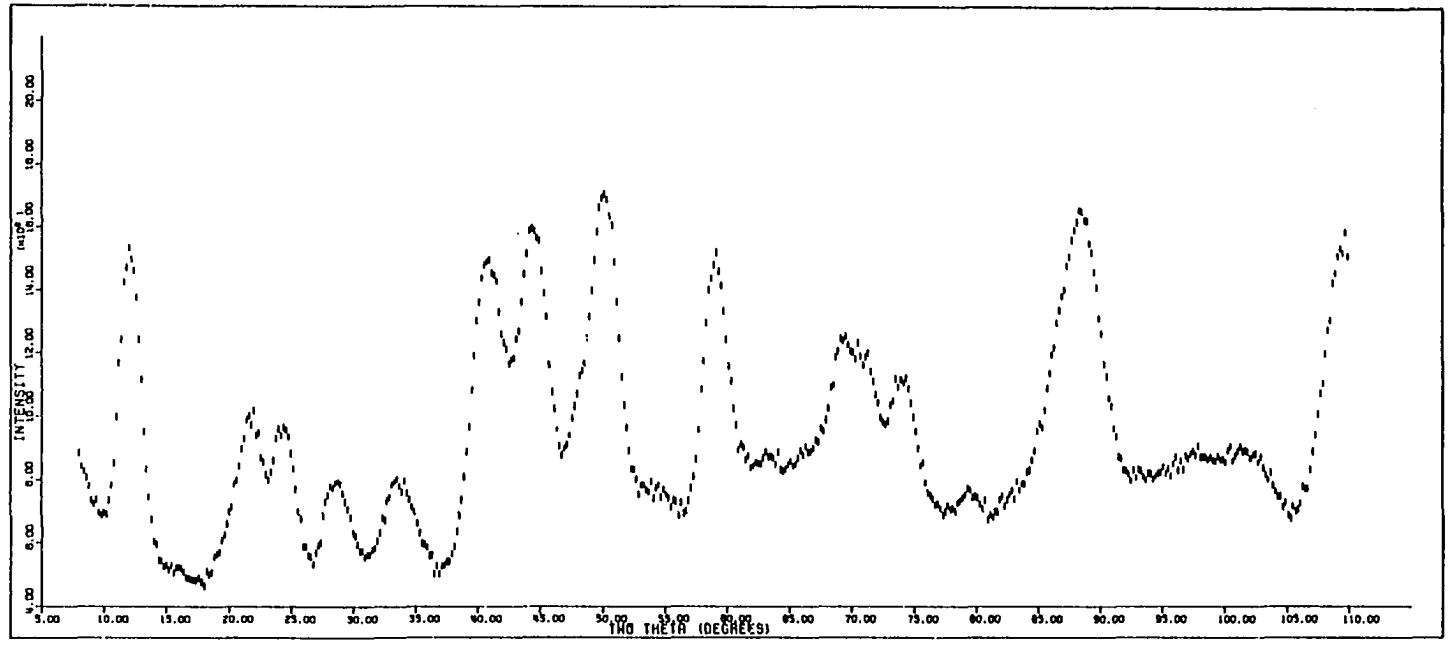

Figure 15. Neutron diffraction pattern of $ZrBrD_{0.5}$ obtained from the multiple wavelength diffractometer at ALRR

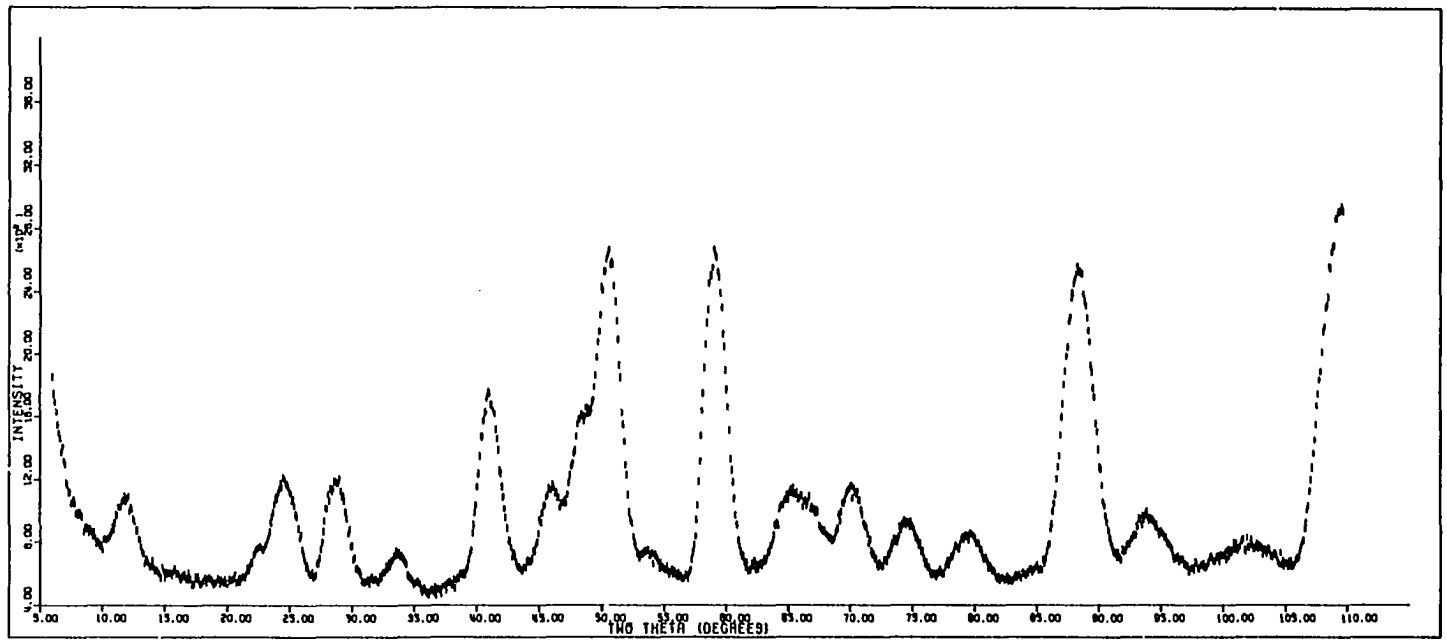

Figure 16. Neutron diffraction pattern of ZrBrD obtained from the multiple wavelength diffractometer at ALRR

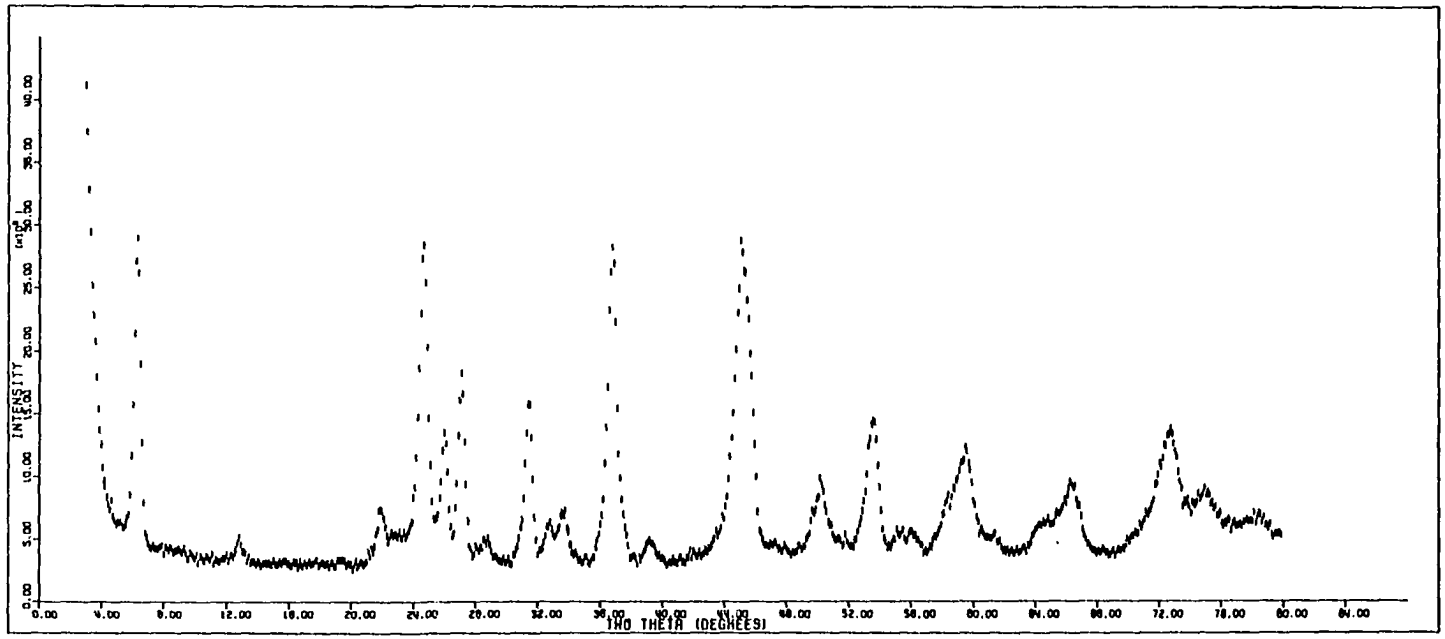

Figure 17. Neutron diffraction pattern of ZrBrD obtained from the single wavelength diffractometer at the University of Missouri